

# **DEVELOPMENT OF POLYMER NANOCOMPOSITES FOR AUTOMOTIVE APPLICATIONS**

A Thesis

Presented to

The Academic Faculty

By

**Chun Chu**

In Partial Fulfillment

Of the Requirements for the Degree

Master of Science in Mechanical Engineering

Georgia Institute of Technology

December, 2010

# **DEVELOPMENT OF POLYMER NANOCOMPOSITES FOR AUTOMOTIVE APPLICATIONS**

Approved By:

Dr. Kyriaki Kalaitzidou  
The George W. Woodruff School of  
Mechanical Engineering  
*Georgia Institute of Technology*

Dr. Jonathan Colton  
The George W. Woodruff School of  
Mechanical Engineering  
*Georgia Institute of Technology*

Dr. Suman Das  
The George W. Woodruff School of  
Mechanical Engineering  
*Georgia Institute of Technology*

Date Approved: September 10<sup>th</sup>, 2010

## ACKNOWLEDGEMENTS

I was fortunate to begin my research as an undergraduate student in Dr. Kyriaki Kalaitzidou's lab in Spring 2008. I was able to gain technical knowledge, experimental skill, and communication skill under the supervision of my advisor Dr. Kalaitzidou. I would like to thank Dr. Kalaitzidou for her guidance and for funding my master program at Georgia Institute of Technology. I would like to thank Honda Motor for funding my research project too.

I would like to thank Dr. Jonathan Colton and Dr. Suman Das for being my committee members and for their assistance with my research including the use of rotary tumbler in Dr. Das' lab, use of impact test equipments, use of UTS machine for tensile test, and use of Mettler Toledo density determination kit from Dr. Colton's lab.

I would like to thank Dr. Samuel Graham for the use of compression molding unit, Dr. Satish Kumar for the use of TMA device for CLTE measurements, Dr. Gleb Yushin for the use of Solartron 1260 and Mechanical Properties Research Lab (MPRL) for the use of three point bending device for flexural test. I would like to thank Mr. Rick Brown from MPRL and graduate student MD Bhuiyan for the assistance with flexural test, undergraduate students Vanessa Tseng, Kent Bartlett, Ashley Stanford, and Juan Lozada, for their assistance with compounding, injection molding, tensile test, impact test, heat distortion temperature measurement, density measurement, stiffness measurement, electrical conductivity measurement and taking SEM images.

I would like to thank all the graduate students in my lab, MD Bhuiyan, Mehdi Kareven and Brian Simpson for their assistance with my coursework and experiments, and their

involvement in lab meetings and discussions. In addition, I would like to thank all the academic faculty and staff in the George W. Woodruff School of Mechanical Engineering.

Finally, I would like to thank my parents, my sister and my brother for their love and support throughout my life.

# TABLE OF CONTENTS

|  |      |
|--|------|
| ACKNOWLEDGEMENTS.....  | iii  |
| LIST OF TABLES.....  | viii |
| LIST OF FIGURES.....   | ix   |
| LIST OF ABBREVIATIONS.....   | xii  |
| SUMMARY.....   | xiii |
| <br>   |      |
| 1. INTRODUCTION.....   | 1    |
| 1.1    Polymer Nanocomposites.....   | 1    |
| 1.1.1 Overview.....  | 1    |
| 1.1.2 Advantages and Limitations of Polymer Nanocomposites.....                | 3    |
| 1.2    Polymer Nanocomposites Demand in Automotive Applications.....           | 5    |
| 1.3    Electrically Conductive Polymer Composites.....                         | 9    |
| 1.3.1 Applications.....  | 9    |
| 1.3.2 Factors Affecting Electrical Conductivity and Percolation Threshold..... | 10   |
| 1.3.3 Percolation Theory.....  | 12   |
| 1.3.4 Electrical Conductivity Models.....                                      | 14   |
| 1.4    Research Objectives.....  | 15   |
| <br>   |      |
| 2. MATERIALS, MANUFACTURING AND CHARACTERIZATION.....                          | 17   |
| 2.1    Materials.....  | 17   |
| 2.2    Manufacturing.....  | 18   |
| 2.2.1 Compounding.....   | 18   |
| 2.2.2 Molding Methods.....   | 20   |
| 2.3    Characterization Methods.....   | 22   |
| 2.3.1 Mechanical Properties.....   | 22   |
| 2.3.2 Thermo-mechanical Properties.....  | 22   |
| 2.3.3 Other Properties.....  | 23   |

|   |    |
|---|----|
| 3. PERFORMANCE CHARACTERIZATION AND COMPARISON OF POLYMER NANOCOMPOSITES.....               | 26 |
| 3.1 Comparison of Compounding Methods for Nanokaolin-PP Nanocomposites.....                 | 27 |
| 3.1.1 Flexural Properties.....  | 27 |
| 3.1.2 Impact Strength.....  | 29 |
| 3.1.3 Heat Distortion Temperature.....  | 30 |
| 3.2 Comparison of Compounding Methods for xGnP-PP Nanocomposites.....                       | 30 |
| 3.2.1 Flexural Properties.....  | 31 |
| 3.2.2 Impact Strength.....  | 32 |
| 3.2.3 Heat Distortion Temperature.....  | 32 |
| 3.3 Performance Comparisons between talc-PP, xGnP-PP, and nanokaolin-PP Nanocomposites..... | 33 |
| 3.3.1 Flexural Properties.....  | 34 |
| 3.3.2 Impact Strength.....  | 36 |
| 3.3.3 Heat Distortion Temperature.....  | 37 |
| 3.3.4 Coefficients of Linear Thermal Expansion.....   | 37 |
| 3.3.5 Stiffness.....  | 39 |
| 3.3.6 Specific Density.....   | 40 |
| 3.4 Morphological Characterization.....   | 41 |
| 3.5 Ashby Plots: Specific Property and Material Cost.....                                   | 43 |
| 3.6 Summary of Results.....   | 49 |
| 3.7 Conclusions.....  | 50 |
| 4. PREDICTING ELECTRICAL CONDUCTIVITY OF POLYMER NANOCOMPOSITES...53                        |    |
| 4.1 Electrical Conductivity of Polymer Nanocomposites.....                                  | 53 |
| 4.2 Rheological Properties.....   | 55 |
| 4.3 Flexural Properties .....   | 57 |
| 4.4 Electrical Conductivity Models and Comparison to the Experimental Data.....             | 59 |
| 4.4.1 Percolation Model.....  | 59 |
| 4.4.2 General Effective Medium Model.....   | 64 |
| 4.4.3 Mamunya’s Model.....  | 65 |

|     |  |    |
|-----|--|----|
| 4.5 | Conclusions.....                                 | 68 |
| 5.  | CONCLUSIONS AND SUGGESTIONS FOR FUTURE WORK..... | 70 |
| 5.1 | Research Conclusions.....                        | 70 |
| 5.2 | Suggestions for Future Work.....                 | 73 |
|     | REFERENCES.....                                  | 74 |

## LIST OF TABLES

|           |  |    |
|-----------|--|----|
| Table 1.1 | Advantages and limitations of polymer nanocomposites.....                          | 5  |
| Table 3.1 | Material Costs.....  | 44 |
| Table 3.2 | Summary of composite performance in various properties.....                        | 49 |
| Table 4.1 | Comparison between experimental data and percolation model (first approach)..      | 61 |
| Table 4.2 | Comparison between experimental data and percolation model (second approach) ..... | 62 |
| Table 4.3 | Comparison between experimental data and GEM model.....                            | 64 |
| Table 4.4 | Comparison between experimental data and Mamunya's model.....                      | 66 |



## LIST OF FIGURES

|            |  |    |
|------------|--|----|
| Figure 1.1 | Comparison of diameters of various fibrous carbon-based materials [4] .....  | 2  |
| Figure 1.2 | Comparison of interphase volume in a composite and nanocomposite.....  | 2  |
| Figure 1.3 | Seatback of 2004 Acura TL [13] .....   | 6  |
| Figure 1.4 | 2005 General Motors Hummer H2 SUT's center bridge, sail panel, and box-rail protector [14] .....                         | 7  |
| Figure 1.5 | Carbon E7 police car [15] .....  | 7  |
| Figure 1.6 | Michelin Krylion carbon tires [18] .....   | 8  |
| Figure 1.7 | Fiber dispersion and alignment caused by (a) injection molding (b) compression molding.....                              | 12 |
| Figure 1.8 | Percolation of a fluid in a porous medium.....   | 13 |
| Figure 1.9 | Typical electrical conductivity trend as a function of filler volume fraction.....                                       | 14 |
| Figure 2.1 | Direct melting mixing procedure.....   | 18 |
| Figure 2.2 | Procedure of the coating method.....   | 19 |
| Figure 2.3 | Injection molding unit.....  | 21 |
| Figure 2.4 | Compression molding set up.....  | 21 |
| Figure 2.5 | Impedance test set up.....   | 24 |
| Figure 3.1 | Flexural strength comparison of nanokaolin-PP prepared with melt mixing, compatibilizer, sonication, and surfactant..... | 28 |
| Figure 3.2 | Flexural modulus comparison of nanokaolin-PP prepared with melt mixing, compatibilizer, sonication, and surfactant.....  | 28 |
| Figure 3.3 | Impact strength comparison of nanokaolin-PP prepared with melt mixing, compatibilizer and sonication.....                | 29 |
| Figure 3.4 | HDT comparison of nanokaolin-PP prepared with melt mixing, compatibilizer and sonication.....                            | 30 |

|             |   |    |
|-------------|---|----|
| Figure 3.5  | Comparison of (a) flexural strength and (b) modulus for 10 wt% xGnP1-PP as a function of compounding method.....      | 31 |
| Figure 3.6  | Impact strength comparison of xGnP1- PP prepared with sonication, melt mixing and tumbling.....                       | 32 |
| Figure 3.7  | HDT comparison of xGnP- PP prepared with sonication, melt mixing and tumbling.....                                    | 33 |
| Figure 3.8  | Flexural strength comparison of talc-PP, xGnP1-PP, xGnP15-PP and nanokaolin-PP .....                                  | 35 |
| Figure 3.9  | Flexural modulus comparison of talc-PP, xGnP1-PP, xGnP15-PP and nanokaolin-PP.....                                    | 35 |
| Figure 3.10 | Impact strength comparison between talc-PP and xGnP1-PP composites at ambient temperature and at low temperature..... | 36 |
| Figure 3.11 | HDT comparison of talc-PP, xGnP1-PP, xGnP15-PP and nanokaolin-PP.....   | 37 |
| Figure 3.12 | CLTE comparison of various composites.....  | 38 |
| Figure 3.13 | Stiffness comparison of PP, talc-PP, xGnP-PP and nanokaolin-PP.....   | 39 |
| Figure 3.14 | Specific density comparison of PP, talc-PP, xGnP-PP and nanokaolin-PP.....  | 40 |
| Figure 3.15 | Fracture surface for 40 wt% talc-PP.....  | 42 |
| Figure 3.16 | Fracture surface of 10 wt% xGnP1-PP.....  | 42 |
| Figure 3.17 | Fracture surface of 10 wt% nanokaolin-PP.....   | 43 |
| Figure 3.18 | Ashby plot of specific flexural strength vs. material cost.....   | 45 |
| Figure 3.19 | Ashby plot of specific flexural modulus vs. material cost.....  | 45 |
| Figure 3.20 | Ashby plot of specific impact strength vs. material cost.....   | 46 |
| Figure 3.21 | Ashby plot of specific HDT vs. material cost.....   | 47 |
| Figure 3.22 | Ashby plot of specific CLTE vs. material cost.....  | 48 |
| Figure 4.1  | Electrical conductivity of CB-PP, VGCF-PP and xGnP15-PP as a function of filler weight percent.....                   | 54 |

|             |  |    |
|-------------|--|----|
| Figure 4.2  | Tan Delta of CB-PP, VGCF-PP and xGnP15-PP as a function of filler weight percent.....            | 56 |
| Figure 4.3  | Viscosity of CB-PP, VGCF-PP and xGnP15-PP as a function of filler weight percent.....            | 56 |
| Figure 4.4  | Flexural strength of CB-PP, VGCF-PP and xGnP15-PP as a function of filler weight percent.....    | 58 |
| Figure 4.5  | Flexural modulus of CB-PP, VGCF-PP and xGnP15-PP as a function of filler weight percent.....     | 58 |
| Figure 4.6  | Linear fitting of experiment data with pre-set filler conductivity for percolation model.....    | 60 |
| Figure 4.7  | Linear fitting of experiment data without pre-set filler conductivity for percolation model..... | 62 |
| Figure 4.8  | Experimental filler conductivity as a function of theoretical filler conductivity...             | 63 |
| Figure 4.9  | Comparison between experimental data and GEM model predictions.....                              | 65 |
| Figure 4.10 | Comparison between experimental data and Mamunya's model predictions.....                        | 67 |

## LIST OF ABBREVIATIONS

|       |   |
|-------|---|
| PNC   | Polymer Nanocomposites                  |
| PP    | Polypropylene                           |
| xGnP  | Exfoliated Graphite Nanoplatelets       |
| NCH   | Nylon-Clay Hybrid                       |
| MWCNT | Multi-Walled-Carbon-Nanotube            |
| HDT   | Heat Distortion Temperature             |
| CLTE  | Coefficient of Linear Thermal Expansion |
| CB    | Carbon Black                            |
| VGCF  | Vapor Grown Carbon Nanofibers           |
| SDS   | Sodium Dodecyl Sulfate                  |
| MW    | Molecular Weight                        |
| MM    | Melt Mixing                             |
| S     | Sonication                              |
| T     | Tumbling                                |
| SEM   | Scanning Electron Microscope            |
| GEM   | General Effective Medium                |
| ROM   | Rule of Mixture                         |

## SUMMARY

Polymer nanocomposites (PNCs) have gained significant interest because they have outstanding performance that allows cost reduction, weight reduction, and product improvement. This research study focuses on the manufacture and characterization of PNCs in order to explore their potential in automotive applications. More specifically, polypropylene (PP) nanocomposites reinforced with xGnP and nanokaolin were fabricated by manufacturing methods that optimize their performances. Exfoliated graphite nanoplatelets (xGnP) are promising nanofillers that are cost effective and multifunctional with superior mechanical, thermo-mechanical and electrical properties. Nanokaolin is a newly introduced natural mineral found in Georgia that has not been studied as of now. PNCs reinforced with these two nanofillers were characterized in terms of mechanical, thermo-mechanical, and various other properties, and then compared to talc-reinforced PP composites, which are the current state of the art for rear bumpers used by Honda Motor. Characterization results indicated that xGnP had better performance than talc and nanokaolin. Furthermore, the addition of xGnP introduces electrical conductivity in the PNCs, leading to more potential uses for PNCs in automotive applications such as the ability to be electrostatic painted. In order to fabricate PNCs with a desired conductivity value, there is need for a design tool that can predict electrical conductivity. Existing electrical conductivity models were examined in terms of model characteristics and parameters, and model predictions were compared to the experimental data. The percolation threshold is the most important parameter in these models, but it is difficult to determine experimentally, that is why a correlation between thermo-mechanical properties and electrical conductivity is also investigated in this study.

# CHAPTER 1

## INTRODUCTION

Polymer nanocomposites have been a popular field in nanotechnology and have gained increasing interest both from academia and industry during the past decades. They have advantageous material properties and can be engineered for a wide range of applications. The automotive industry seeks to maximize the potential use of PNCs in order to tackle environmental concerns, cost reduction, and product differentiation. This chapter aims to give an overview of the background, advantages, limitations, and current applications of PNCs in the automotive industry. This study particularly emphasizes electrically conductive PNCs, as electrical properties are highly important in many of the most advanced technologies including automobiles. Applications of electrically conductive PNCs, and the theory and modeling of electrical conductivity are introduced in the next sections. This chapter serves to provide the motivation, challenges and interests that lead to the goals and objectives of this research study.

### **1.1 Polymer Nanocomposites**

#### 1.1.1 Overview

This study investigates PNCs for engineering applications. The term PNCs implies a material combination of at least two distinct phases, with a polymer matrix and one nano-sized filler material (at least one dimension below 100 nm) [1]. Research and development in nanocomposites in terms of theory, manufacturing, properties characterization, and potential applications have thrived since the proposal of a nylon 6-clay hybrid composite by Toyota in 1987 [2,3]. Theoretical and experimental investigations have been performed on metallic,

ceramic, and polymeric matrices with emphasis on the last one. Nanofillers of interest include both organic materials such as carbon particles (graphite, carbon nanofibers and carbon black) and inorganic materials such as nanoclays. The most common carbon fillers and their diameters are shown in Figure 1.1 [4]

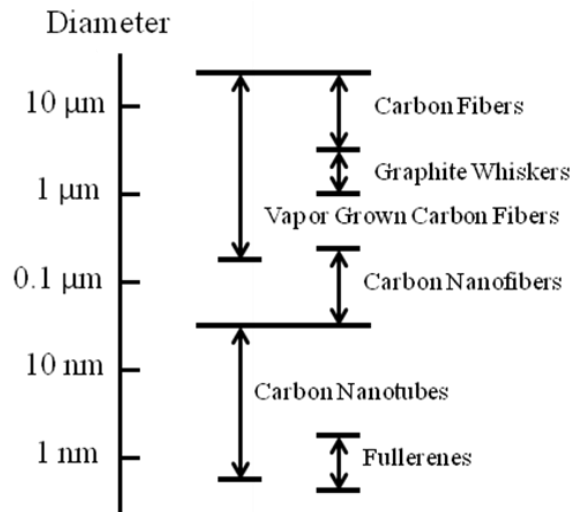


Figure 1.1 Comparison of diameters of various fibrous carbon-based materials [4]

PNCs have smaller filler size, and therefore have higher surface to volume ratio compared to composites reinforced with micro-sized fillers. This leads to higher surface to volume ratio as shown in Figure 1.2. Perfect contact at the polymer and filler interface is critical for the transfer of mechanical load, thermal conductivity, and electrical conductivity.

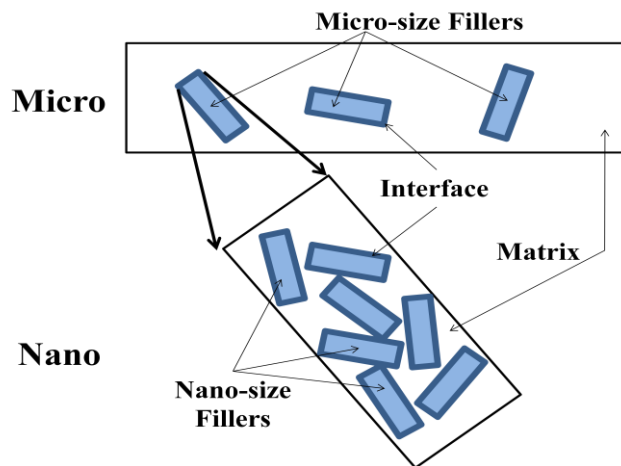


Figure 1.2 Comparison of interphase volume in a composite and a nanocomposite

### 1.1.2 Advantages and Limitations of Polymer Nanocomposites

The concept of multifunctional PNCs is based on a number of the enhanced material properties exhibited, and on advantages over other materials such as metals and plastics that can be obtained in certain applications by altering the volume fraction of filler particles. In addition, PNCs, as all polymeric composites, have the advantage of desirable properties, including resistance against corrosion, noise damping, and thermal stability over metallic materials. The selection of polymers as the matrices allows PNCs to be low in cost and density, to be ductile, and, to be easy to manufacture. A low density enables lower weight and thus lower energy consumption within electronics and machinery components; these qualities can boost performance, enhance efficiency, and save cost. PNCs hold another advantage; they can be fabricated through various rapid and precise manufacturing methods such as injection molding, compression molding, vacuum-bag molding, contact-molding and resin transfer molding [5]. Thermoplastic PNCs have low melting points and attain low viscosity allowing molding of more complex geometries. Superior electrical properties can also be achieved with the use of conductive fillers. Consider a simplified equation [6] for calculating the distance between the filler particles:

$$s = d \left[ \left( \frac{\pi}{6\phi_v} \right)^{1/3} - 1 \right] \quad (1.1)$$

where  $s$  is the interparticle distance,  $d$  is the particle diameter,  $\phi_v$  is volume fraction of equal-size spherical particles on a lattice. This equation indicates that the interparticle distance is proportional to the particle diameter. Therefore, the use of conductive nanofillers can yield lower percolation threshold in the material as compared to conventional fillers. The percolation threshold is the minimum amount of filler required to introduce electrical conductivity in the



composite by forming a conductive network with the polymer. The advantages of PNCs will be further described and illustrated with specific practical examples in the applications section.

In the development of PNCs, there are challenges and limitations to be accounted for. There are trade offs in material properties as the filler amount within the polymeric system increases. Even though the moduli of PNCs increase with increasing filler content, their toughnesses, and thus their impact strengths decrease, as the materials become more brittle. The viscosities of PNCs also increase with the filler content and manufacturing is more difficult with higher viscosity [7]. In addition, a highly viscous flow of the polymer melt may induce large forces or cause short shots during extrusion and injection molding. Furthermore, uniform dispersion of the filler particles within the polymer matrix is also difficult at high filler content due to formation of agglomerates, which also can act as site defects limiting the mechanical performance of PNCs. As shown by Equation 1.1, smaller interparticle distance is preferred for electrical conductivity; however, smaller interparticle distance leads to poor wetting of the filler by the polymer due to the limited mobility of the polymer chains around the nanofillers.

As a summary, Table 1.1 provides an overview of general advantages and limitations in the use of PNCs.

Table 1.1 Advantages and limitations of polymer nanocomposites

| <b>Advantages</b>   | <b>Limitations</b>  |
|---|---|
| <ul style="list-style-type: none"> <li>• Improved mechanical properties (strength and modulus)</li> <li>• Structural and thermal stability</li> <li>• Electrical conductivity (with conductive fillers)</li> <li>• Corrosion resistance</li> <li>• Noise damping</li> <li>• Lower permeability of fluids (with specific fillers)</li> <li>• Low density (relatively to metallic/ceramic materials)</li> <li>• Low cost (only for low filler content or inexpensive fillers)</li> <li>• Ease of manufacturing</li> </ul> | <ul style="list-style-type: none"> <li>• Difficulty in uniform dispersion</li> <li>• High viscosity with high amount of filler</li> <li>• Formations of agglomerates</li> </ul> |

## 1.2 Polymer Nanocomposites Demand in Automotive Applications

Rising fuel costs and environmental issues in the 21st century have raised concerns for buyers, sellers and manufacturers in the automotive industry. In the US, the current

administration has requested the automotive industry to improve fuel-consumption efficiency from the current standard of 25 mpg to 35 mpg by 2016 [8]. PNCs are seen as one of the means to solve the following issues: improving fuel-consumption efficiency (more miles per gallon), reducing greenhouse gas emission, and reducing manufacturing costs. These issues have become primary objectives for the automotive industry. The first application was from a research group at Toyota Motor, which developed a nylon-clay hybrid (NCH) nanocomposite with improved performance in modulus and heat distortion temperature which was used in timing belt covers as part of the engine [9]. Since then clay reinforced PNCs have been widely used in automotive products including exterior panels, interiors panels, step-assist, and engine parts [10, 11]. General Motors has been using PNCs in their automobiles since 2002; step-assists of the 2002 Safari and Astro vans were molded from a polyolefin nanocomposite reinforced with 2.5% nanoclay replacing the 15% talc-PP composite [12], these changes have resulted in 7%-8% weight reduction, higher impact strength at low temperature, and improved part surface quality. A PP nanocomposite also appeared on the seatbacks of the 2004 Honda Motors' Acura TL as shown by Figure 1.3 and on the body side molding of the 2004 General Motors' Chevrolet Impala [13]. The 2005 General Motors Hummer H2 SUT had a cargo bed with seven pounds of PNCs for its center bridge, sail panel, and box-rail protector [13,14]. General Motors is now using about 299,371 kg of nanocomposites per year [14].



Figure 1.3 Seatback of 2004 Acura TL [13]



Figure 1.4 2005 General Motors Hummer H2 SUT's center bridge, sail panel, and box-rail protector [14]

Taking this a step further, Carbon Motors Corporation has announced that the world's first police car to be coated with 100% Fluorex® Paintfilm on a thermoplastic exterior developed by Soliant, LLC will be on duty in 2012 as shown in Figure 1.5 [15]. This purpose-built police car "E7" is designed to have body panels covered by those nanocomposite paintfilms to demonstrate resistance against weathering, chemical reactions, chips, dings, and dents. Apart from enhanced properties, the use of paintfilm reduces cost by eliminating traditional painting. The traditional paint line often accounts for up to 40% of the cost of a new auto production plant along with space occupation and other environmental consequences [16]. Another example of Soliant's paintfilm application is the replacement of chrome-painting for various motor companies. According to Soliant, the film meets various OEMs' (Original Equipment Manufacturer) specifications on UV protection and scratch resistance. Honda's 2008 Odyssey is another example of the use of Fluorex paintfilm on body side and rocker molding.



Figure 1.5 Carbon E7 police car [15]

PNCs are also used in tire products today. A project report from The U.S Department of Energy stated that the use of PNCs was able to decrease energy loss to hysteresis by nearly 20% compared to a styrene-butadiene rubber sample with no nanofillers. It was estimated that a 20% reduction in rolling resistance could lead to a 4% saving in fuel consumption and a similar amount of reduction in greenhouse gas emissions. By converting all the tires of U.S. cars into PNC tires, it is possible to reduce fuel consumption by more than 4 billion gallons and to reduce carbon dioxide emission by more than 22 million tons annually [17]. Apart from automobile tires, Michelin also has products of bicycle tires utilizing nanoparticles. Krylion Carbon has a center thread reinforced with nano sized carbon black as shown in Figure 1.6 below, resulting in a 30% or more increase in durability [18].



Figure 1.6 Michelin Krylion carbon tires [18]

Applications of fuel cells in automobiles have gained significant research interest in the automotive industry recently. Electrically conductive PNCs can be used as bipolar plates in fuel cells and to eliminate the need for painting. More applications of electrically conductive PNCs will be elaborated in the next section.

## **1.3 Electrically Conductive Polymer Composites**

### 1.3.1 Applications

The addition of conductive fillers to polymers, especially carbon materials such as carbon black, carbon fiber, graphite and carbon nanotubes, enables the PNC to be electrically conductive [8]. The demand for such conductive materials has been growing in various technological applications. In the automotive industry, electrostatic painting and bipolar plates in fuel cells are the two major applications. Other applications include flexible electronics and packaging, electrostatic dissipation, electrostatic shielding, and electromagnetic interference shielding [19].

For auto buyers, one of the common expectations for vehicles is an optically smooth surface to achieve an aesthetically pleasing appearance. In the past, paint on its own had poor adhesion to the target, poor durability, and provided little protection of the target object. For this purpose, many companies such as Honda Motor use a paint product called “Primer” on their automobiles to counter the issues mentioned above [20]. However, direct electrostatic painting can be utilized instead of a primer if the parts are composed of electrically conductive PNCs. Electrostatic painting is a commercial process where charged paint particles are sprayed onto the target object, which has to be electrically conductive. This process allows more uniform and better controlled thickness during the painting. The attractions between the paint particles and the electrically conductive parts enable strong adhesion and minimize overspray of the paint by drawing the paint droplets to the rear of the part with a phenomenon called “wrap” [21], which also reduces environmental impact by controlling the emission of volatile organic compounds in paint [22]. This process and the employment of electrically conductive PNCs may thus replace the use of primer in certain automotive applications to reduce cost and weight. In 1997, electrically conductive PNCs were also used to produce Ford Taurus and Mercury Sable mirror

housings along with this process. GE plastics and Hyperion Catalysis, Inc. also produced a multi-walled-carbon-nanotube (MWCNT) conductive resin for an electrostatic painting process developed by United Technologies Automotives [21].

Fuel cells are one of the most revolutionary technologies in the energy field, as they are “green” energy sources with high power densities, low operation temperatures (for certain types of fuel cells) [23], and they convert hydrogen fuel into water as the only by product. In order to generate an appropriate amount of power, individual fuel cells must be linked together to form a fuel cell stack. A bipolar plate is the component in fuel cells that serves this key linkage function. For current fuel cells, the most commonly used material for bipolar plates is graphite due to its corrosion resistance, low bulk density and high electrical conductivity [24-26]. The problem arises with the difficulty of machining flow channels in the bipolar plate when using graphite [27]. The bipolar plate is the fuel cell component with the highest cost (around 38% of the cost of a fuel cell stack [28]), and this motivates a need to find another suitable material in order to save time and cost. Manufacturing PNCs by using processes such as injection molding or compression molding is also less difficult and costly as compared to machining graphite. Furthermore, one study showed that a MWCNT-based nanocomposite bipolar plate has lower ohmic resistance than graphite bipolar plates. This results in improved fuel cell performance at the median current density region [29].

### 1.3.2 Factors Affecting Electrical Conductivity and Percolation Threshold

Both the polymer matrix and the conductive fillers strongly affect the percolation threshold and electrical conductivity. Factors involved include material intrinsic properties, filler shape, filler size, and surface interactions between polymer and filler. Each conductive filler has

its own intrinsic electrical conductivity, which dictates the maximum electrical conductivity of the corresponding PNCs. Different shapes produce different aspect ratios (the ratio of larger to smaller dimension, typically length to diameter). It has been shown that the higher the aspect ratio, the lower the percolation threshold [30-32].

For spherical fillers, size is another factor that affects percolation threshold [33], because smaller particle size means higher interface volume as mentioned in the introduction of this chapter. This allows easier transfer of electrons and aids the formation of a conductive network. The filler-polymer interactions also have an effect on electrical conductivity and percolation threshold. The interactions are dictated by the surface energies of two materials. According to Mamunya's study, a smaller difference in the two surface energy values indicates better wetting [34], which also indicates better dispersion and less agglomeration of filler particles resulting in higher electrical conductivity and lower percolation threshold.

Lastly, studies have shown that dispersion and orientation of the filler, which is defined by the manufacturing method and processing conditions used to make the PNCs, strongly affect the electrical conductivity [35-40]. First, the compounding method, such as sonication or melt mixing, and the use of compatibilizer, will determine the level of filler wetting by the polymer, the agglomeration, and dispersion. Furthermore, molding methods such as injection molding and compression molding can affect the filler alignment as illustrated Figure 1.7 (a), which shows the possible orientation and alignment of fibers dispersed within the polymer by injection molding, and Figure 1.7 (b) shows the possible orientation and alignment achieved by compression molding.



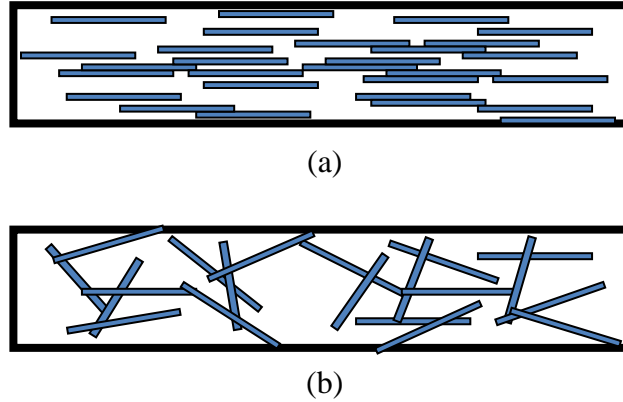


Figure 1.7 Fiber dispersion and alignment caused by (a) injection molding (b) compression molding

It is concluded that injection molded PNCs have a higher percolation threshold due to the alignment of particles in one direction as compared to the random dispersion obtained by compression molding. In addition, the alignment in one direction also leads to anisotropic electrical conductivity of PNCs, where electrical conductivity measured along the alignment of the fibers is greater than that measured perpendicular to the direction of alignment.

### 1.3.3 Percolation Theory

When the filler content of PNCs reaches a critical loading level, or percolation threshold, a conductive network is formed within the polymer. Such a formation is described by the percolation theory introduced by Hammersley and Broadbent in 1957 [41]. The percolation process was defined as the spread of a “fluid” through a “medium” with a random mechanism and in a statistical manner. One example from their study is the flow of fluid through a number of atoms connected with bonds as illustrated in Figure 1.8. The probability of the bond being “dammed” is  $p$ , or the probability for being “undammed” is  $q = 1 - p$ . A fluid may flow through the undammed bonds only. For a given  $p$ , there is a possibility that the fluid may flow

from the top to the bottom of the medium. In the case of electrical conductivity of PNCs, the amount of filler content may be seen as the probability of the bond being undammed (for the electrons to “flow through”) and the polymer matrix may be seen as the porous medium.

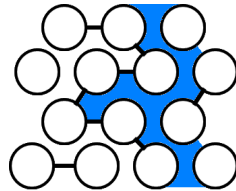


Figure 1.8 Percolation of a fluid in a porous medium

Figure 1.8 illustrates a typical electrical conductivity trend of composites reinforced with conductive fillers as function of filler volume fraction. There are mainly three stages in this curve. At low filler content, filler materials dispersed in the polymer are not in contact with each other, and electrons cannot be transferred through the bulk of the composites due to the insulating nature of the polymer. Generally, the composite’s electrical conductivity before the percolation threshold is similar to that of neat polymer as displayed in region A. However, as filler content increases, the material system reaches its percolation threshold, which means that the filler particles begin to contact each other, forming a conductive network within the composite, causing the composites electrical conductivity to increase drastically as shown in region B. The region between the two red dotted lines in Figure 1.9 is defined as the percolation regime. Further addition of filler does not have any significant effect on increasing electrical conductivity due to the completion of a conductive network at the percolation threshold and the system reaches a plateau conductivity level as indicated in region C.

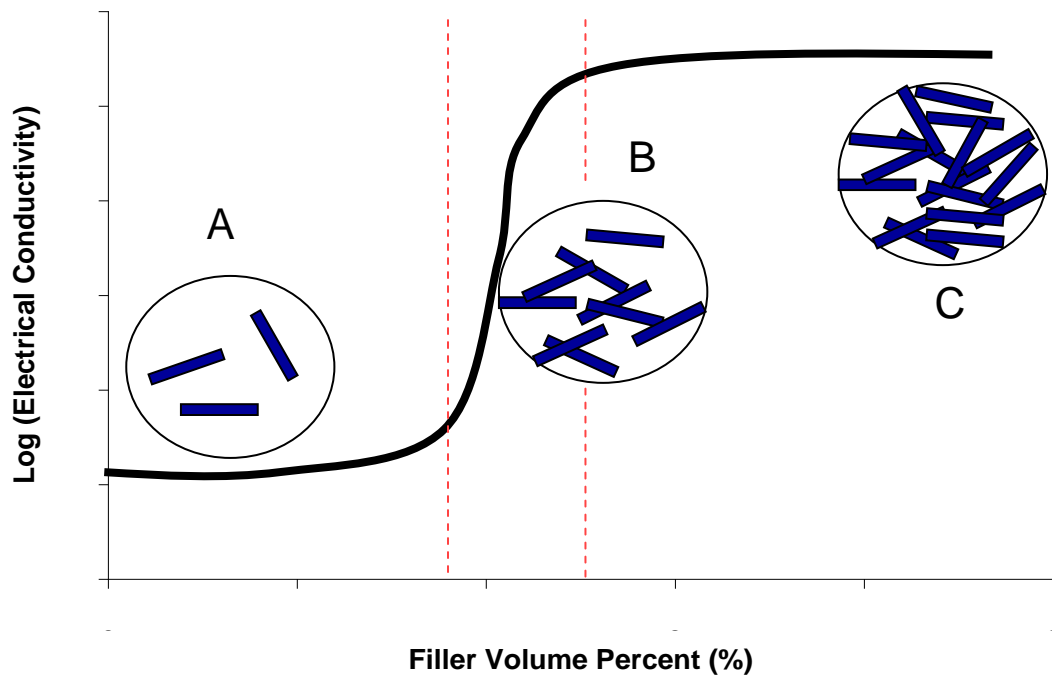


Figure 1.9 Typical electrical conductivity trend as a function of filler volume fraction

#### 1.3.4 Electrical Conductivity Models

There are various applications for electrically conductive PNCs, as discussed previously, and each application requires a specific electrical conductivity value. However, it is difficult to determine the exact amount of filler required for a targeted electrical conductivity value. Fabricating the composites at each filler loading level is not efficient as a solution in engineering practice. Therefore, there is need for a design tool that predicts electrical conductivity. Many theoretical models have been proposed for this purpose. There are four major classes of electrical conductivity models found in the literature including statistical, thermodynamic, geometrical, and structure-oriented models as discussed by Lux [42]. Each model considers certain factors that affect electrical conductivity. Statistical models take into account on the probability of contacts between filler particles. Thermodynamic models consider the interfacial interactions

between the matrix and the filler. Geometrical models consider the filler's size and shape and structure-oriented models account for the physical differences such as filler orientation as introduced by processing methods.

Existing models do not account for all the factors that affect electrical conductivity as discussed. This makes the models unreliable, as there are infinite combinations of matrix, filler, and processing methods that can be used. Moreover, most of these models require an input of the percolation threshold [33,43-45]. However, there is no existing method that can determine this directly. The current approach is to fabricate the composites at different filler loading levels, which is costly and time consuming.

#### **1.4 Research Objectives**

The existing and potential applications discussed provide the motivation for developing advanced PNCs. This study aims to develop a PNC that has promising performance for automotive applications by examining different compounding methods and characterizing various composite properties. Specifically, the objectives of this study are to:

1. Manufacture talc reinforced composites (the current state of the art for rear bumper used by Honda Motor) as a function of filler loading level;
2. Manufacture PNCs reinforced with different nanofillers as a function of filler loading level utilizing various compounding methods;
3. Characterize and compare the performance of the composites made in (1) and (2) in terms of:
  - Flexural properties
  - Impact strength

- Heat distortion temperature (HDT)
  - Coefficient of linear thermal expansion (CLTE)
  - Stiffness
  - Specific Density;
4. Manufacture electrically conductive PNCs as a function of filler loading level;
  5. Explore any potential correlation between percolation threshold, flexural properties and rheological properties by characterization of PNCs fabricated in (4); and
  6. Investigate electrical conductivity models and understand their assumptions and limitations. Compare model predictions to experimental data using the PNCs made in (4).

## CHAPTER 2

### MATERIALS, MANUFACTURING AND CHARACTERIZATION

This chapter covers the details of the materials used, and the compounding and molding methods employed for the fabrication of PNCs. Materials include the polymer matrix and five different fillers. Five compounding methods and two molding methods were utilized to fabricate the specimens. The specimens were fabricated and characterized as a function of filler loading level. Characterization methods for mechanical properties, thermo-mechanical properties, electrical conductivity, and specific density are also described in this chapter.

#### 2.1 Materials

The polymer used is PP homopolymer in pellet form (Pro-fax HP564S) and in powder form (Pro-fax 6301) supplied by LyondellBasell. The powder consisted of particles with diameters in the range of 100  $\mu\text{m}$  to 300  $\mu\text{m}$ . PP homopolymer is used for this study for two main reasons: PP is used as the polymer matrix in many automotive applications; it does not have a functional group, so there are no chemical interactions with the fillers, which simplifies the study. The fillers used are carbon black (CB), vapor grown carbon nanofibers (VGCF), exfoliated graphite nanoplatelets (xGnP1 and xGnP15), nanokaolin, and talc. Carbon black (Ketjenblack, EC600JD, by Akzo Novel Polymer Chemicals LLC) is composed of spherical particles with diameters ranging from 10 nm to 30 nm and has electrical conductivity of 10-100 S/cm. Vapor grown carbon nanofibers (Pyrograf-III: PR-19, XT-LHT by Pyrograf Products, Inc.) have lengths from 50  $\mu\text{m}$  to 100  $\mu\text{m}$ , average diameter of 150nm and electrical conductivity of 10,000 S/cm. Two types of exfoliated graphite nanoplatelets (xGnP) provided by XG sciences

are used, both have the same thickness of approximately 10nm, xGnP1 has an average diameter of 1 $\mu$ m, xGnP15 has an average diameter of 15 $\mu$ m, and they have electrical conductivities of 18,000 S/cm. Nanokaolin was supplied by Imerys and talc powder was provided by Honda; no additional information for these materials is available due to proprietary issues.

## 2.2 Manufacturing

### 2.2.1 Compounding

Three compounding methods were used to disperse the nanofillers within the polymer matrix: direct melt mixing, solid state mixing with a tumbler, and coating with sonication. Additionally, compatibilizer and surfactants were used to improve the dispersion for the case of nanokaolin.

#### 2.2.1.1 Direct Melt Mixing

Direct melt mixing was performed by manually mixing the polymer and filler and then feeding the mixture into a twin screw extruder. The materials were mixed at a speed of 250 RPM for 3 minutes at 180 $^{\circ}$ C by two screws as shown in Figure 2.1. The extruder barrel has a volume capacity of 15cc and the maximum force that can be applied is 10 kN during the mixing process.

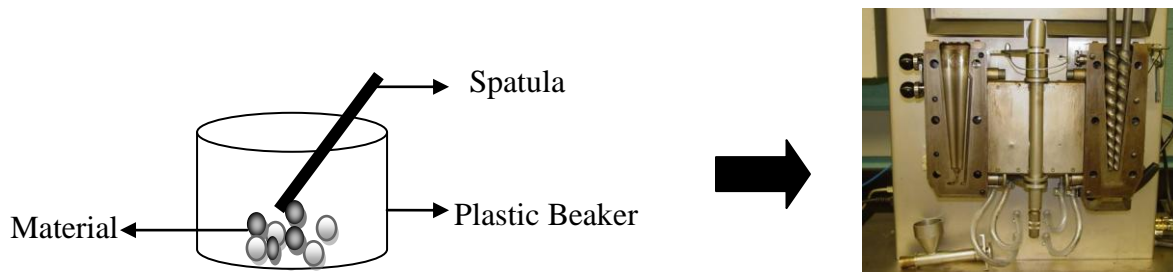


Figure 2.1 Direct melting mixing procedure

### 2.2.1.2 Solid State Mixing Using a Tumbler

xGnP1 and PP were placed in a rotary tumbler (cylindrical vessel) from U.S. Stoneware. 1/3 of the tumbler's volume was filled with spherical zirconium milling media with a 5 mm diameter manufactured by Glenmills, Inc. and then xGnP1 and PP were filled up to half of the tumbler's volume. The vessel then was rotated at 150 RPM for 48 hours. Once mixing was completed, the xGnP-PP mixture was fed into the extruder after the removal of milling media by using a sieve.

### 2.2.1.3 Coating with Sonication

This compounding method has been developed especially for xGnP nanocomposites [46]. The procedure is summarized in Figure 2.2.

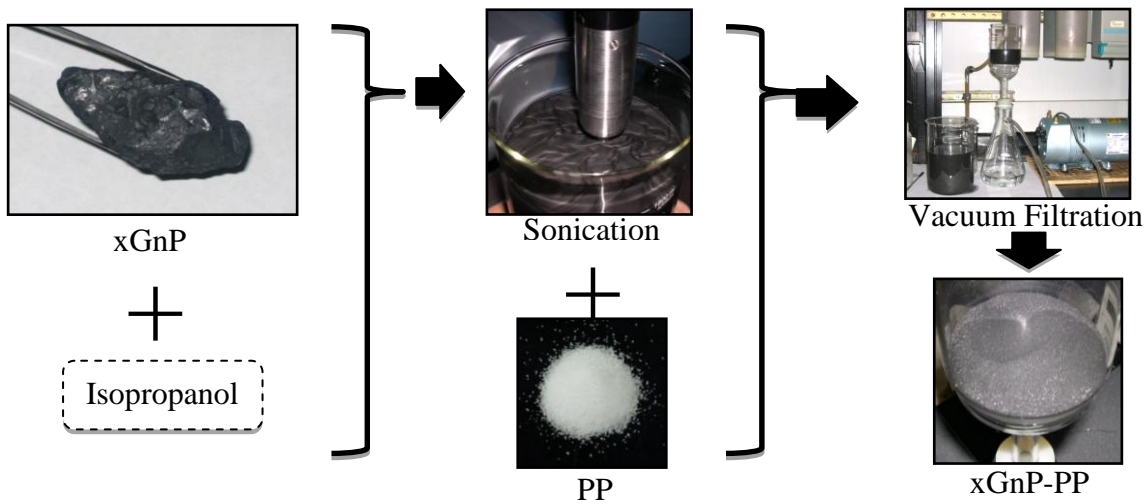


Figure 2.2 Procedure of the coating method

First, xGnP was immersed in isopropanol inside a glass beaker and ultrasonic waves were applied by a sonicator to break down xGnP agglomerates into individual platelets for 40 minutes.



PP powder was added to the solution during the last 10 minutes of sonication. Vacuum filtration using a pump was employed to filter out the alcohol and to obtain the xGnP coated PP powder. The coated PP was left to dry and fed into the extruder.

#### *2.2.1.4 Use of Compatibilizer*

For the case of nanokaolin, polypropylene-grafted-maleic anhydride (Sigma Aldrich, MW~9100 g/mol, maleic anhydride 8-10 wt%) was used as a compatibilizer to enhance the filler-polymer interactions and avoid agglomeration of nanokaolin particles. Once the compatibilizer was added the same procedure for direct melt mixing was applied.

#### *2.2.1.5 Use of Surfactants*

Another approach to improve the dispersion of nanokaolin within PP powder is to use surfactants. The surfactant employed was sodium dodecyl sulfate (SDS),  $\text{CH}_3(\text{CH}_2)_{11}\text{OSO}_3\text{Na}$ , water soluble salt by VWR. Sonication was applied to the solution containing water, nanokaolin and SDS at a weight ratio of 1/3 for 15 minutes. Sonication was applied for another 15 minutes after the addition of PP and the water was filtered out by vacuum filtration. To remove the last trace of water, the mixture was heated inside an oven at 70°C. Temperature above 100 °C would soften the material, so a range of lower temperature (60-80°C) could be used. The average (70°C) was used, even though drying might be slower. The dried mixture of nanokaolin, surfactant, and PP was then fed into the extruder.

### 2.2.2 Molding Methods

#### *2.2.2.1 Injection Molding*

Specimens of bars, discs, and dog bones were fabricated by injection molding. Regardless of which compounding method was used, the composite powder was fed through the extruder to be melted as this was the only method for the specimens to be injection molded. The melt was injected at 180°C (same as mixing temperature) and the mold temperature was 80°C. The pressure applied during the process was 53.8 KPa. The injection molding unit used is shown in Figure 2.3.



Figure 2.3 Injection molding unit

#### 2.2.2.2 Compression Molding

In order to fabricate specimens in the form of thin film, compression molding was performed using the injection molded specimens (to avoid any alternation in dispersion of the filler). The platens were heated to 200°C and the aluminum plates were used to avoid platens contamination. The two platens were brought in contact but no pressure was applied for 5min until the specimens melted. A force of 4448N was applied for 5 minutes. A schematic of the process is shown in Figure 2.4. The produced films were cooled to ambient temperature by water cooling at an average rate of 1°C/s.

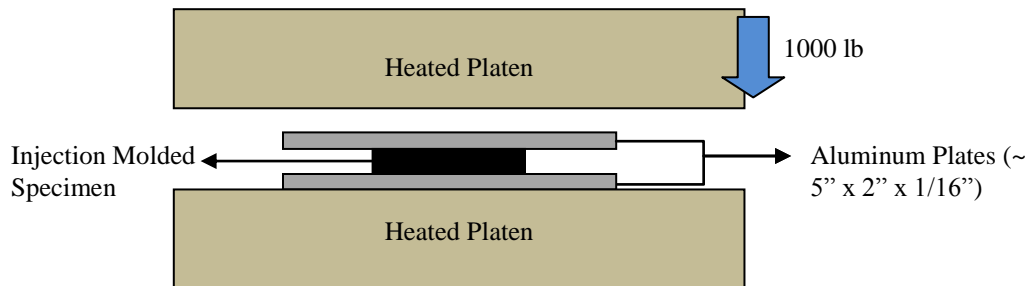


Figure 2.4 Compression molding set up

## **2.3 Characterization Methods**

### 2.3.1 Mechanical Properties

Flexural strength and modulus were determined by three point bending according to ASTM D790. The test was performed at a test speed of 1.27 mm/min, using a preload of 5N by a mechanical testing equipment by MTI Instruments Inc.

A notched Izod Impact test was performed for bar shaped specimens according to ASTM D256 standard. The specimens were notched at a notch depth of 2.54 mm, and clamped into the impact test fixture with the notch facing the striking direction of the pendulum. The impact test was performed at ambient temperature and at a low temperature. For low temperature tests, the specimens were stored inside a freezer set to -20°C for 24 hours.

### 2.3.2 Thermo-mechanical Properties

Heat distortion temperature (HDT) was measured with a dynamic mechanical analyzer (Q800 by TA Instruments) according to ASTM D648 Standard (stress of 0.455 MPa). The deflection of the specimen was measured with a temperature ramp at a rate of 2°C/min at three point bending mode.

The coefficient of linear thermal expansion (CLTE) was determined using a thermo-mechanical analyzer (TMA Q400 by TA Instruments) according to ASTM D696. Thin compression molded films were tested from -20 °C to 45 °C at rate of 5 °C/min with nitrogen cooling and with a preload of 0.003N. The CLTE was determined at the temperature regime higher than the glass transition temperature, which is identified as the transition point of two linear regimes in the measurement curve.

Tan Delta (loss modulus/storage modulus) and dynamic viscosity were measured using a rheometer (ARES 2000 by TA Instruments) with parallel plate geometry set up. A dynamic strain sweep was performed to identify the range of strain in the elastic region. Then Tan Delta and dynamic viscosity were determined from a dynamic frequency sweep analysis at 175°C, 1% strain and frequency of 0.251 Hz.

Stiffness was determined by a DMA operating at single cantilever mode. The specimen was first heated to a constant temperature of 35°C for 5 min to avoid any temperature gradient; following this it was heated up to 145°C at a rate of 3 °C/min.

### 2.3.3 Other Properties

A two probe impedance test was performed with a Solartron 1260 with the voltage set to 0.30 mV and the resistance measured at a frequency of 0.1 Hz. The two probe method has also been used for measuring composites resistance in various studies [47-49]. The specimens tested were cut from the middle portion of the flex bars made by injection molding and had average dimensions of 0.5 x 1.28 x 0.33 (cm). Silver conductive paste was applied to the cross sections (1.28 x 0.33) of the specimen to ensure perfect contact with the electrodes. The resistance was measured along the 0.5 cm direction with electrodes (alligator clips) clipped on the copper tapes as shown in Figure 2.5.

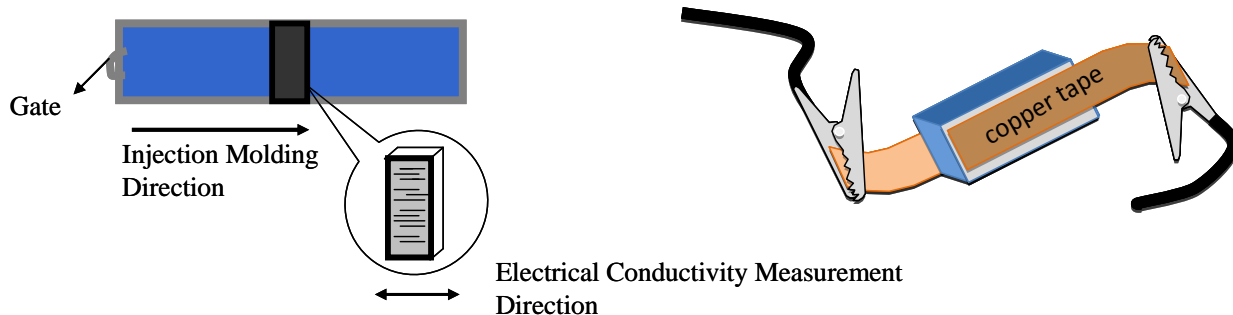


Figure 2.5 Impedance test set up

The resistance of CB-PP, VGCF-PP and xGnP15-PP was measured as a function of filler loading level and electrical conductivity was determined based on the following equations:

$$\rho = \frac{RA}{l} \quad (2.1)$$

$$\sigma = \frac{1}{\rho} \quad (2.2)$$

where  $R$  is the specimen resistance in  $\Omega$ ,  $A$  is the cross sectional area in  $\text{cm}^2$ ,  $l$  is the length in  $\text{cm}$ ,  $\rho$  is the resistivity in  $\Omega\text{-cm}$  and  $\sigma$  is the conductivity in  $\text{S/cm}$ .

Specific density was measured by a Mettler Toledo density determination kit. Water was used as the reference liquid. The water temperature was measured during the experiment, and its density at that specific temperature was obtained from a reference table. The mass of the specimen in air and in water was obtained with the balance. Specific density was determined with Equation 2.3,

$$\rho = \frac{A}{P} \rho_0 \quad (2.3)$$

where  $\rho$  is the specimen density,  $A$  is the specimen mass in air,  $P$  is the specimen mass in water and  $\rho_0$  is the density of water at the corresponding temperature. In order to improve the accuracy

of the results, a correction is applied to Equation 2.3 to account for the air buoyancy as shown in Equation 2.4,

$$\textit{Calculated Density} + 0.0012 \frac{\textit{g}}{\textit{cm}^3} \textit{Air Buoyancy} = \textit{Effective Density} \quad (2.4)$$

# **CHAPTER 3**

## **PERFORMANCE CHARACTERIZATION AND COMPARISON OF POLYMER NANOCOMPOSITES**

PP based composites reinforced with talc (talc-PP) were compared to composites reinforced with xGnP (xGnP-PP) and nanokaolin (nanokaolin-PP). Studies on xGnP nanocomposites have shown that xGnP was a promising filler material for composites in terms of mechanical, thermo-mechanical, and electrical properties [50,51]. On the other hand, nanokaolin is a new product by Imerys that has never before been used as a filler material in PP. In this chapter, talc-PP, xGnP-PP and nanokaolin-PP were fabricated and characterized in terms of mechanical properties, thermo-mechanical properties, and specific density. However, investigation of the effects of compounding methods on xGnP-PP and nanokaolin-PP was performed in order to optimize the performance before the comparison to talc-PP.

Although talc-PP at 40 wt% is the current state of the art for the rear bumper used by Honda, performance comparisons between xGnP-PP, nanokaolin-PP and talc-PP were not made at 40 wt% because xGnP cost at least 25 times more than talc. Nanokaolin is a new product that is not supplied at commercial quantity currently and its cost remains unknown. Apart from cost, the emphasis is on comparison of 10 wt% composites also because agglomerations may have negative effects on performance for filler loadings higher than 10 wt%, according to data from Figure 4.4 (data obtained beforehand) and reference [50].

Lastly, Ashby plots are presented in order to give a summary of composite performance with respect to specific properties and cost.

### **3.1 Comparison of Compounding Methods for Nanokaolin-PP Nanocomposites**

Four types of compounding methods were applied to disperse nanokaolin in PP: melt mixing (MM), coating method/sonication (S), compatibilizer use (1.5 wt% and 3 wt%), and surfactant use (3:1 surfactant/nanokaolin). The compounding method that optimizes the performance of nanokaolin-PP was determined based on the characterization of properties.

#### 3.1.1 Flexural Properties

Based on the results of the flexural strength and modulus testing shown in Figure 3.1 and Figure 3.2, respectively, melt mixing is the most suitable compounding method for nanokaolin-PP. Sonication produced similar results as melt mixing in terms of flexural strength and modulus. This indicates that the additional step of sonication is not effective in dispersing nanokaolin. The use of 1.5% compatibilizer resulted in lower improvement in flexural strength. However, the use of 3% compatibilizer actually resulted in reduction of both flexural strength and modulus at 3 wt% and 5 wt% nanokaolin. This is possibly due to the replacement of high molecular weight (MW) PP by low MW maleated PP. The reduction in strength overrides the effect of better dispersion. The use of compatibilizer did not show any promising results; however, only one type of maleated PP was used in this study. More research is needed to identify the best compatibilizer for the nanokaolin-PP system. The use of surfactant also resulted in reduction in both flexural strength and modulus at 10 wt% of nanokaolin compared to the neat PP. The reasons are likely to be the low MW of surfactants and the weak interaction between PP and surfactants as PP is non-polar but not hydrophobic. These issues could override the effect of better dispersion.



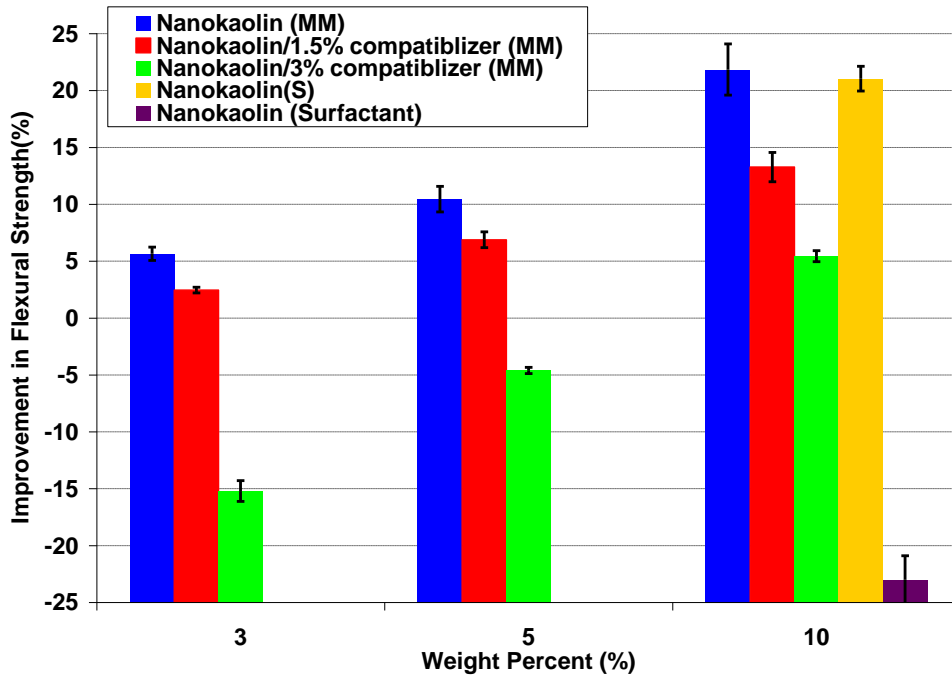


Figure 3.1 Flexural strength comparison of nanokaolin-PP prepared with melt mixing, compatibilizer, sonication, and surfactant

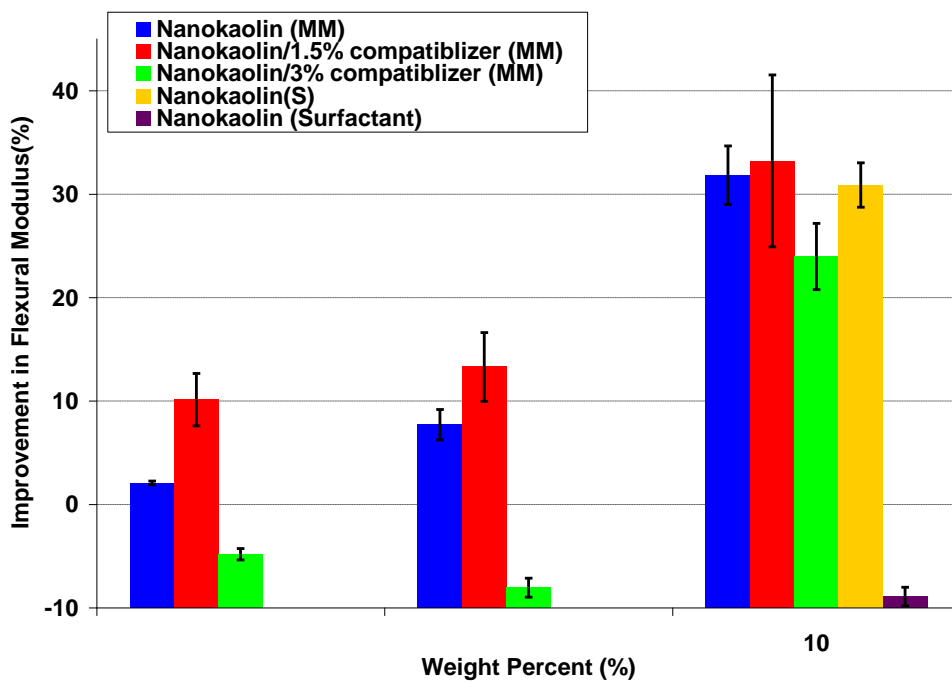


Figure 3.2 Flexural modulus comparison of nanokaolin-PP prepared with melt mixing, compatibilizer, sonication, and surfactant

### 3.1.2 Impact Strength

Figure 3.3 shows the results for comparison of impact strength for nanokaolin-PP. Due to overlapping error bars, no definite conclusion can be drawn from these results. However, 5 wt% and 10 wt% nanokaolin-PP with melt mixing have higher average values than others.

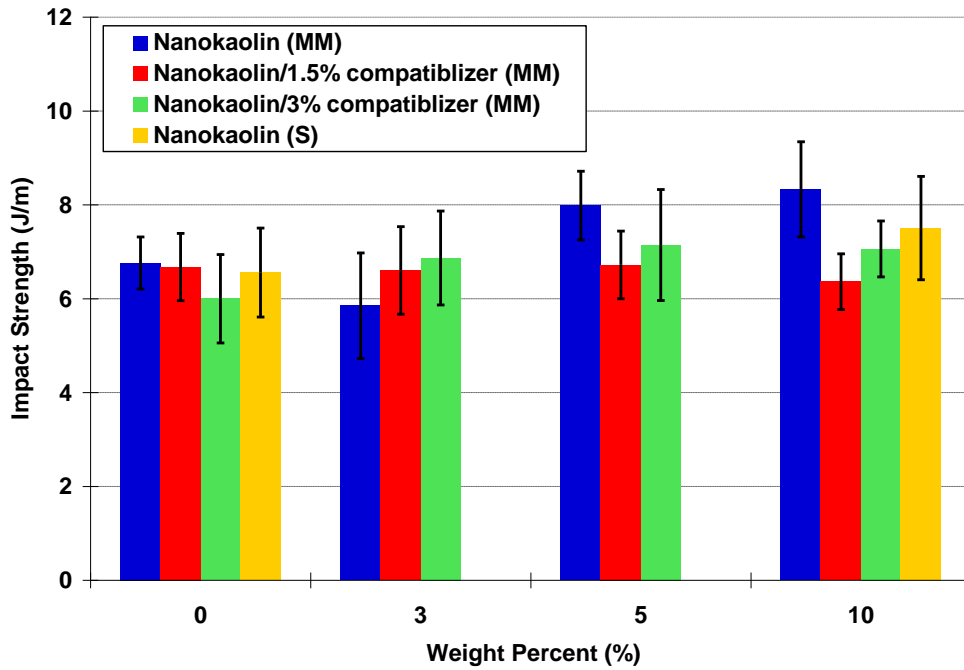


Figure 3.3 Impact strength comparison of nanokaolin-PP prepared with melt mixing, compatibilizer and sonication

### 3.1.3 Heat Distortion Temperature

The comparison of nanokaolin-PP made with melt mixing, 1.5% compatibilizer, 3% compatibilizer and sonication is shown in Figure 3.4. From the results, melt mixing is once again the compounding method resulting in the highest % improvement at all nanokaolin loadings used.

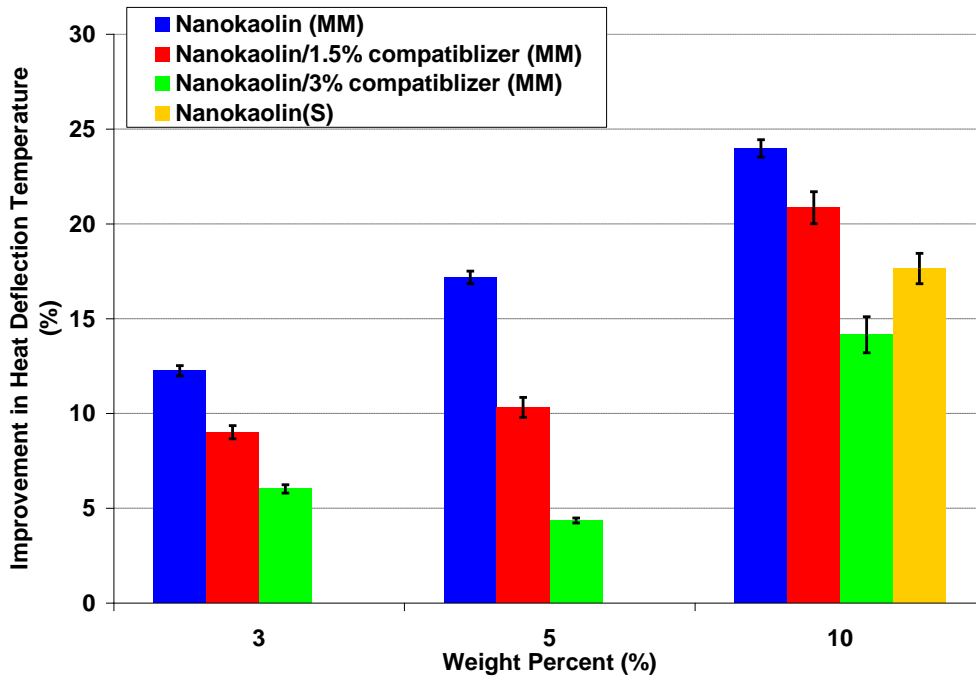


Figure 3.4 HDT comparison of nanokaolin-PP prepared with melt mixing, compatibilizer and sonication

### 3.2 Comparison of Compounding Methods for xGnP-PP Nanocomposites

Three types of compounding methods were applied to disperse xGnP1 in PP (xGnP1-PP): melt mixing (MM), coating method/sonication (S), and solid state mixing using a tumbler (T). The comparison of properties between xGnP1-PP made by different compounding methods was only done at 10 wt% of xGnP1 because this filler concentration would give the most representative results on the effects of compounding due to cost and agglomeration issues.

### 3.2.1 Flexural Properties

The flexural strength and modulus of xGnP1-PP made by three different compounding methods are summarized in Figure 3.5. From the results, the coating method for xGnP1-PP gives a 46% improvement in flexural strength, which is significantly greater than the 25% improvement by melt mixing and solid state mixing with a tumbler. Furthermore, the coating method at 5 wt% xGnP1 gives higher flexural strength than other methods. The same trend is observed for flexural modulus such that the coating method results in over 90% improvement compared to 76% improvement by melt mixing and 51% improvement by tumbling. For both strength and modulus data from xGnP1(S) series, doubling the filler concentration (from 5 wt% to 10 wt%) also doubles the percentage improvement.

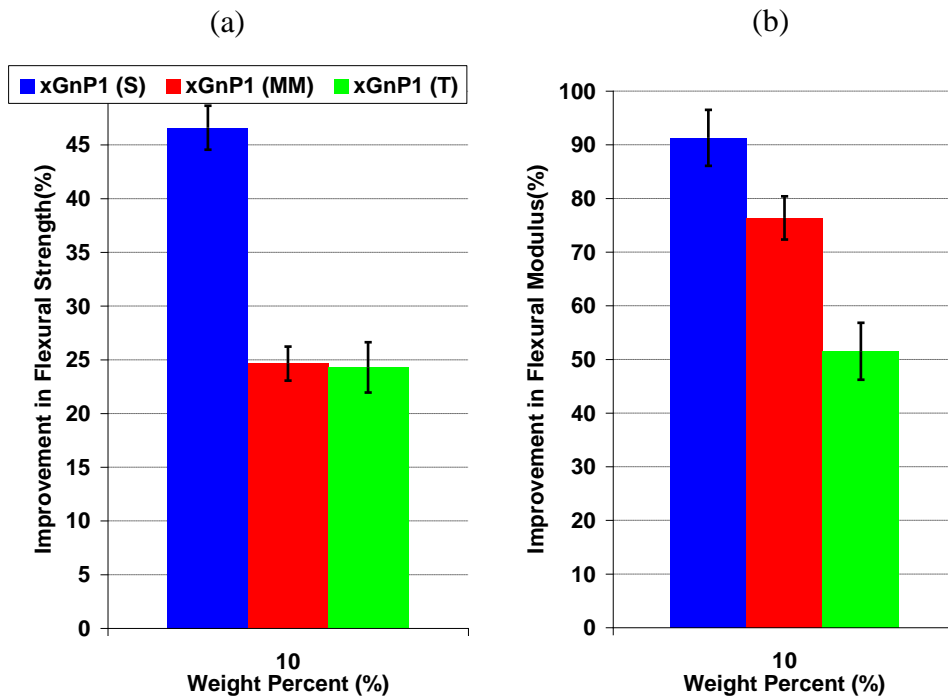


Figure 3.5 Comparison of (a) flexural strength and (b) modulus for 10 wt% xGnP1-PP as a function of compounding method

### 3.2.2 Impact Strength

Figure 3.6 summarizes testing results for impact strength of xGnP1-PP prepared using the various compounding methods.

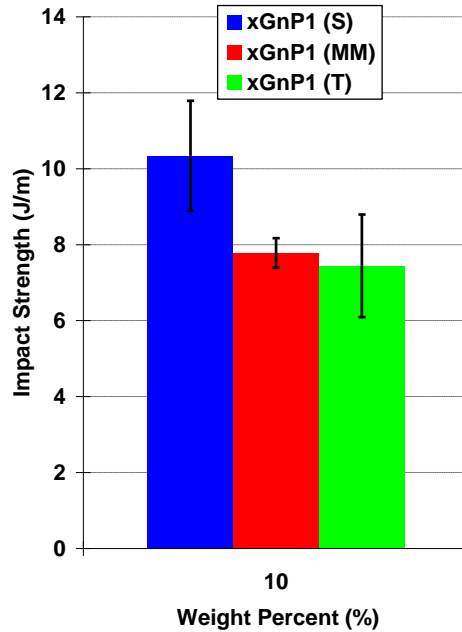


Figure 3.6 Impact strength comparison of xGnP1- PP prepared with sonication, melt mixing and tumbling

Sonication is again the method that gives the best performance. It is also observed that tumbler results are similar or of lower performance compared to the results obtained with melt mixing. Therefore it can be suggested that the use of the tumbler has little or negative effect in the mechanical properties of xGnP1-PP as shown in Figures 3.5-3.7.

### 3.2.3 Heat Distortion Temperature

HDT shows a trend similar to flexural strength. Sonication results in the largest improvement (42%) as compared to roughly 30% improvement resulting from both melt mixing and tumbling as shown in Figure 3.7. In addition, 5 wt% xGnP1-PP made by sonication also

results in same level of performance as compared to the 10 wt% composites made by melt mixing and tumbling.

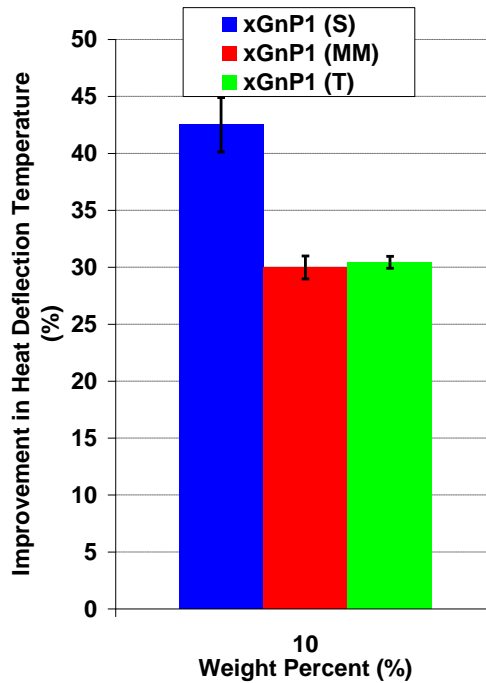


Figure 3.7 HDT comparison of xGnP1- PP prepared with sonication, melt mixing and tumbling

### 3.3 Performance Comparisons between talc-PP, xGnP-PP, and nanokaolin-PP

#### Nanocomposites

According to sections 3.1 and 3.2, the compounding method that optimizes the performance of xGnP1-PP is coating/sonication and it is melt mixing for nanokaolin-PP. In this section these PNCs are compared to talc-PP in terms of mechanical properties, thermo-mechanical properties, and specific density. Talc-PP is used for rear bumper applications, so its mechanical performance is critical. Furthermore, the goal of this study is to develop PNCs for automotive applications and one of the most significant advantages of PNCs is multifunctionality, including, but not limited to, structural, thermal, and electrical performance.

Therefore, it is also crucial to consider thermo-mechanical properties for automotive parts such as fuel tanks and body panels where temperature varies greatly. Additionally, specific density, which is directly related to weight reduction in automobiles, is also determined.

### 3.3.1 Flexural Properties

Comparison of flexural strength and modulus for talc-PP, xGnP-PP, and nanokaolin-PP as a function of filler concentration are shown in Figure 3.8 and Figure 3.9, respectively. The addition of xGnP1 at 3 wt%, 5 wt%, and 10 wt% improved the flexural strength more than the addition of talc, xGnP15, and nanokaolin at equivalent filler content. At 10 wt% of xGnP1 gives 46% improvement, which is significantly higher, almost twice the improvement caused by other fillers. Furthermore, 10 wt% of xGnP1 results in an equal or greater improvement compared to that caused by other fillers at higher loadings. It is also observed that there is no significant improvement in flexural strength upon further addition of xGnP15 from 3 wt% to 10 wt% indicating the presence of agglomerations which cancel out the positive effect that filler addition has on flexural strength. It is noted that composites with filler loadings higher than 10 wt% were only made for xGnP15 because it is the conductive filler with the highest aspect ratio and the goal is to create electronically conductive composites (see Chapter 4). Nanokaolin-PP resulted in the lowest improvement for 3 and 5 wt% loading, but this is still greater than xGnP15 and is comparable to that of 10 wt% talc-PP. In the case of flexural modulus, the addition of xGnP1 resulted in the highest improvement and nanokaolin resulted in the lowest improvement compared to other fillers at similar filler loadings.

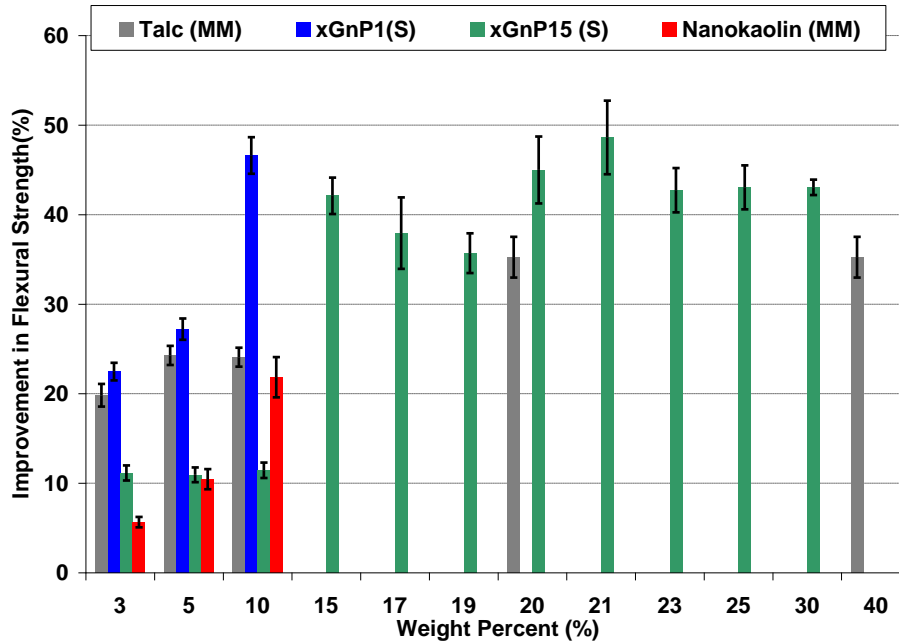


Figure 3.8 Flexural strength comparison of talc-PP, xGnP1-PP, xGnP15-PP and nanokaolin-PP

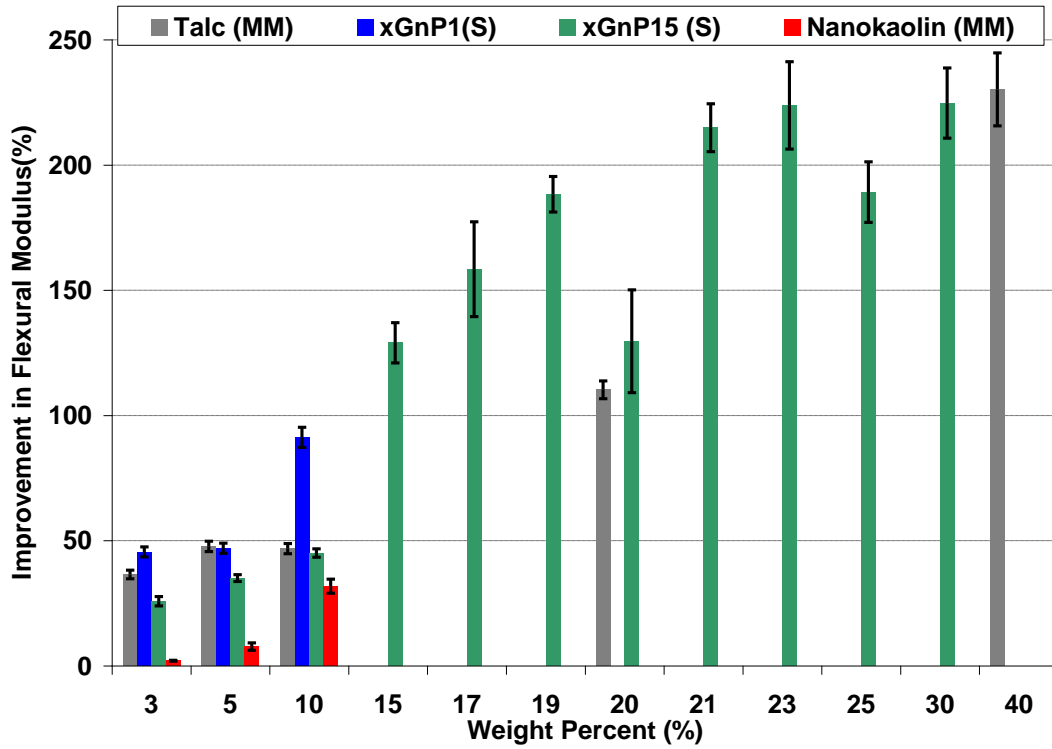


Figure 3.9 Flexural modulus comparison of talc-PP, xGnP1-PP, xGnP15-PP and nanokaolin-PP



### 3.3.2 Impact Strength

It is straight forward that flexural properties are important for automotive applications. In the case of rear bumper application, impact strength is the most critical.

The impact strength of talc-PP and xGnP1-PP was compared at ambient temperature (~22°C) and at low temperature (-20°C) as a function of filler loading as shown in Figure 3.10. It is observed that the addition of 3 wt% xGnP1 increases the impact strength and that no further improvement is observed for further addition of xGnP1. Addition of talc decreases the impact strength especially at higher loadings. The same trends are seen for both temperature conditions. Therefore, xGnP1-PP has significantly higher performance than talc-PP in terms of impact strength. In Figure 3.10, the impact strengths of xGnP15-PP and nanokaolin-PP were not included in the comparison because the specimens were accidentally destroyed and extra materials were not available to fabricate new specimens.

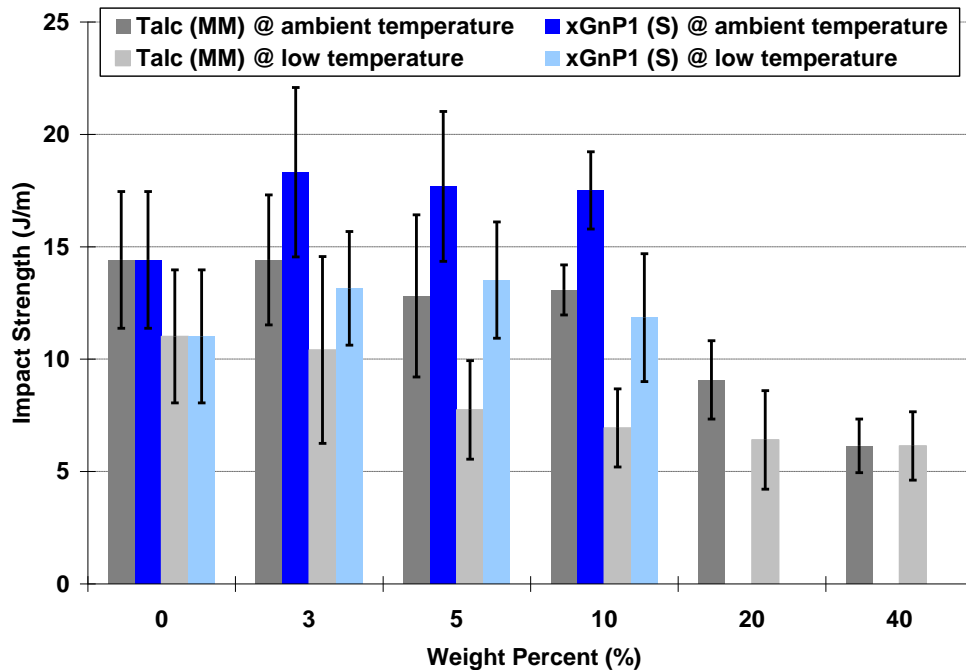


Figure 3.10 Impact strength comparison between talc-PP and xGnP1-PP composites at ambient temperature and at low temperature

### 3.3.3 Heat Distortion Temperature

HDT indicates the maximum temperature a material can reach under a specified deformation and load. A comparison of HDT for talc-PP, xGnP-PP, and nanokaolin-PP is shown in Figure 3.11. Generally, HDT increases with filler content. Again, xGnP1-PP grants the largest improvement (42%) compared to other fillers at all equivalent filler loadings, whereas addition of nanokaolin results in the least improvement.

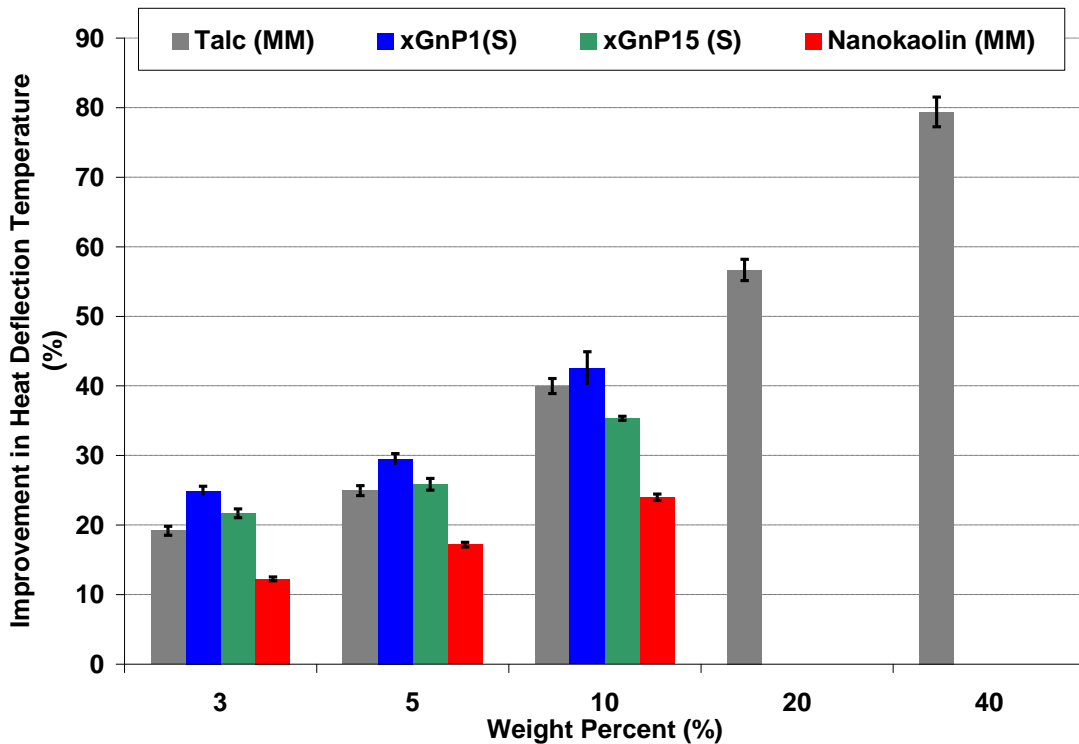


Figure 3.11 HDT comparison of talc-PP, xGnP1-PP, xGnP15-PP and nanokaolin-PP

### 3.3.4 Coefficients of Linear Thermal Expansion

CLTE indicates the amount of shrinkage of a material as a function of temperature. Figure 3.12 shows CLTE of PP and various composites at different filler wt%. xGnP1 reduces the CLTE of PP the most as compared to other filler materials at 10 wt%. Nanokaolin and

xGnP15 composite have the highest CLTEs at 10 wt% loading level. Also, 5 wt% of xGnP1 reduces the CLTE close to the value of talc at 10%.

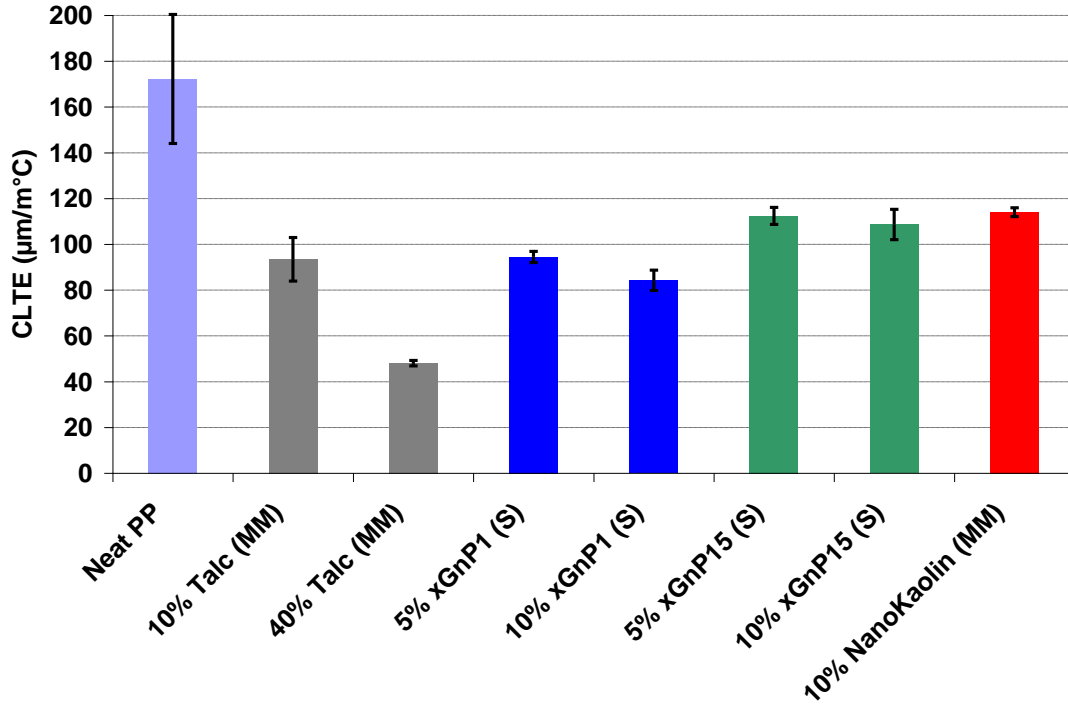


Figure 3.12 CLTE comparison of various composites

The main reasons that xGnP1 results in the largest CLTE reduction compared to other fillers at the same wt% include small size of xGnP1 and good dispersion in the polymer matrix. Small size allows greater polymer-filler interfacial area and it is at the interface where the filler constrains the polymer chains from expanding upon heat. Lastly, more uniform dispersion and few agglomerations due to the sonication used in case of xGnP1 ensure high polymer-filler interface.

### 3.3.5 Stiffness

The stiffness of PP, xGnP-PP, nanokaolin-PP, and talc-PP were measured with DMA in single cantilever mode and the results are shown in Figure 3.13. It was observed that all composites have stiffnesses higher than the neat PP with xGnP15-PP resulting in the largest increase in stiffness for 10 wt% filler filling, followed by xGnP1-PP, talc-PP, and then nanokaolin-PP. At higher temperatures the difference in stiffness due to addition of xGnP1 and xGnP15 vanishes. This is due to the fact that mobility of polymer chains increases at higher temperature. The presence of smaller but more xGnP1 has more dominant effect on stiffness than the presence of larger but fewer xGnP15 platelets. 10 wt% nanokaolin-PP has the lowest stiffness among all composites. Lastly, the coating method has little effect on xGnP1-PP in terms of stiffness as Figure 3.13 indicates for the case of xGnP1-PP made by melt mixing and by the coating method.

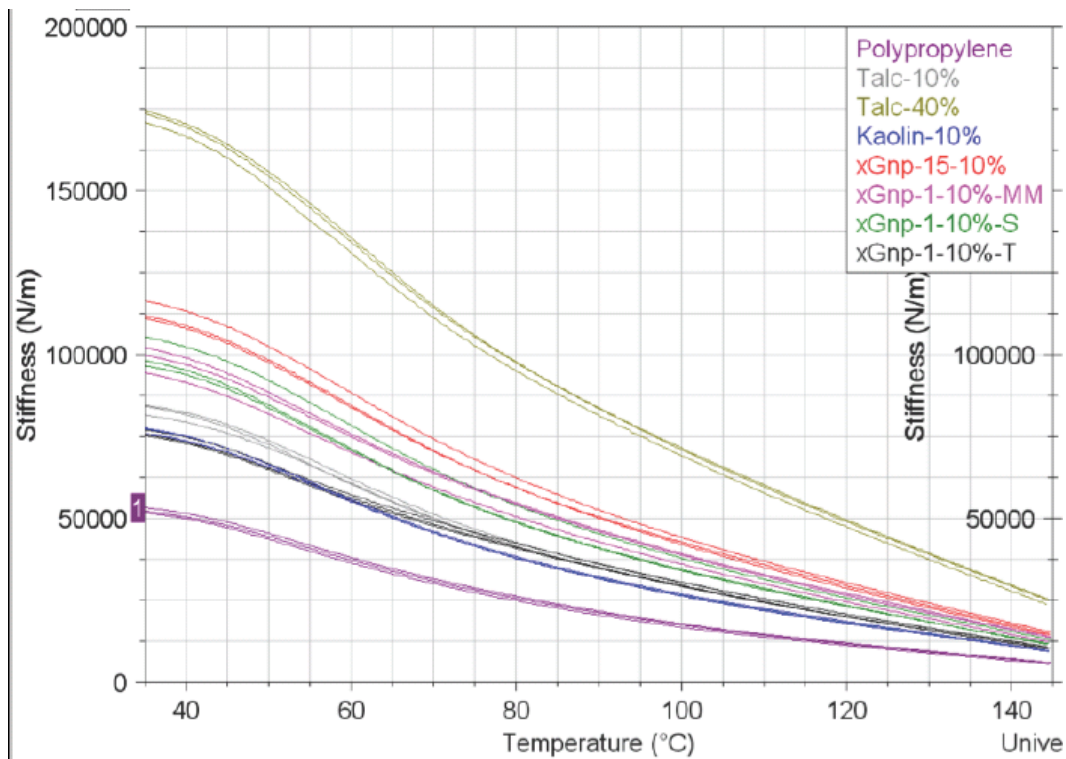


Figure 3.13 Stiffness comparison of PP, talc-PP, xGnP-PP and nanokaolin-PP

### 3.3.6 Specific Density

The specific densities of PP and various composites are shown in Figure 3.14. From the results it is clear that addition of 10 wt% talc increases the specific density significantly compared to addition of 10 wt% xGnP1. Although it was expected that xGnP1 and xGnP15 would lead to same level of specific density, the results indicate that addition of 10% xGnP15 led to slightly higher specific density compared to 10% xGnP1. The experimental data were compared to theoretical composite densities calculated by Rule of Mixture (ROM) as shown in Equation 3.1,

$$\rho_m = \rho_p v_p + \rho_f v_f \quad (3.1)$$

where  $\rho_m$  is the composite density,  $\rho_p$  is the polymer density,  $\rho_f$  is the filler density,  $v_p$  is the polymer volume fraction and  $v_f$  is the filler volume fraction.

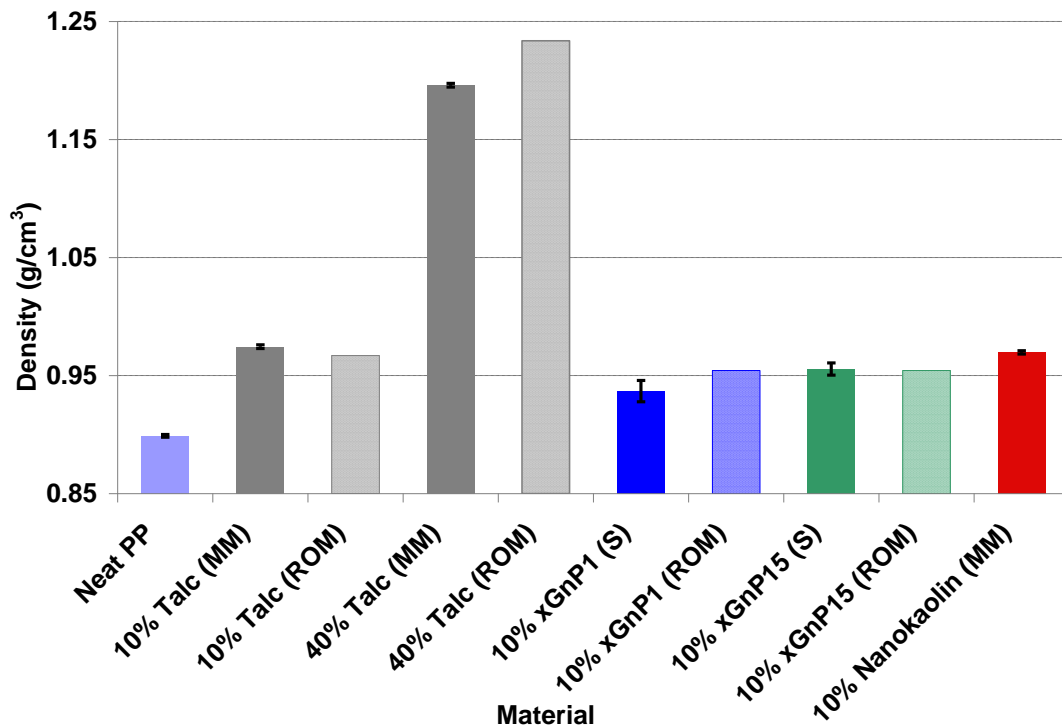


Figure 3.14 Specific density comparison of PP, talc-PP, xGnP-PP and nanokaolin-PP

The densities of PP and xGnP are  $0.902 \text{ g/cm}^3$  and  $2.0 \text{ g/cm}^3$ , respectively. Densities of talc and nanokaolin were not provided by the material supplier. A literature value of  $2.75 \text{ g/cm}^3$  for talc is used [52] in the calculation. As nanokaolin is a new product, there is no reliable source of its theoretical density; hence it is not included in the ROM calculation.

The theoretical values are similar to the experimental values overall. In the case of 40 wt% talc-PP, where a larger difference exists, one reason is that the literature value used may not be the same as the actual density of talc in this study; another possible reason may be due to the existence of cracks and voids in the specimen as shown in Figure 3.15.

### **3.4 Morphological Characterization**

This section includes a series of scanning electron microscope (SEM) images of the fracture surfaces of talc-PP, xGnP-PP and nanokaolin-PP obtained in order to examine the state of dispersion of filler within PP, average size of filler, presence of agglomerates and defects in the composites.

Figure 3.15 shows the fracture surface of 40 wt% talc-PP made by melt mixing and injection molding. The existence of cracks as indicated by the red arrow indicates that addition of talc causes the composite to become brittle and thus leads to low impact strength. The talc platelets coming out of the plane indicate that they are not fully embedded in PP due to weak interactions with and poor wetting by the PP.

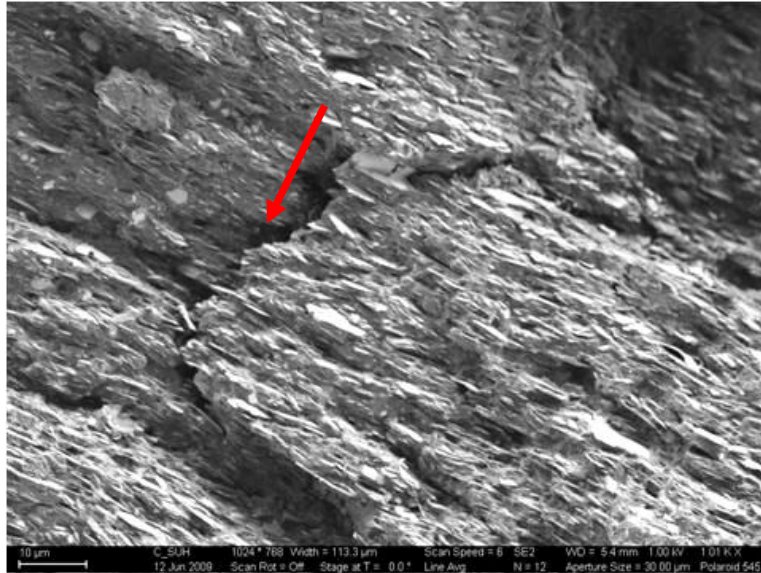


Figure 3.15 Fracture surface for 40 wt% talc-PP

Figure 3.16 shows the fracture surface of 10 wt% xGnP1-PP made by the coating method. xGnP1 has theoretical thickness of 10nm. However, it can be seen from Figure 3.16 that xGnP1 has a thickness of at least 100 nm as pointed by the red arrows. Even with the coating method, it is expected that at high filler loading (10 wt% or higher), there is not enough polymer to separate the individual xGnP from each other and hence agglomeration is unavoidable.

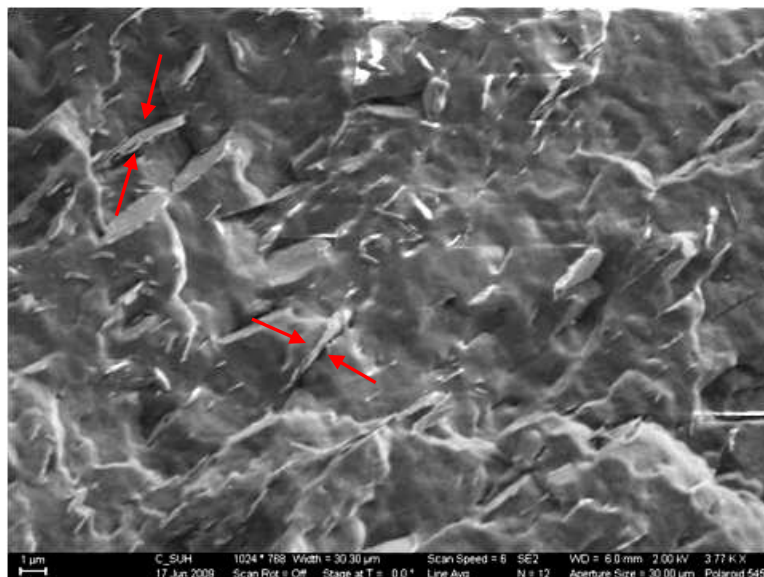


Figure 3.16 Fracture surface of 10 wt% xGnP1-PP

Figure 3.17 shows the fracture surfaces of 10 wt% nanokaolin-PP made by melt mixing and injection molding. It is observed that the dispersion of nanokaolin in PP is uniform. However, the size of individual nanokaolin platelets is in the nano meter range and it is not clear from this SEM if there is dispersion of individual platelets or if there are agglomerates, which would compromise the performance.

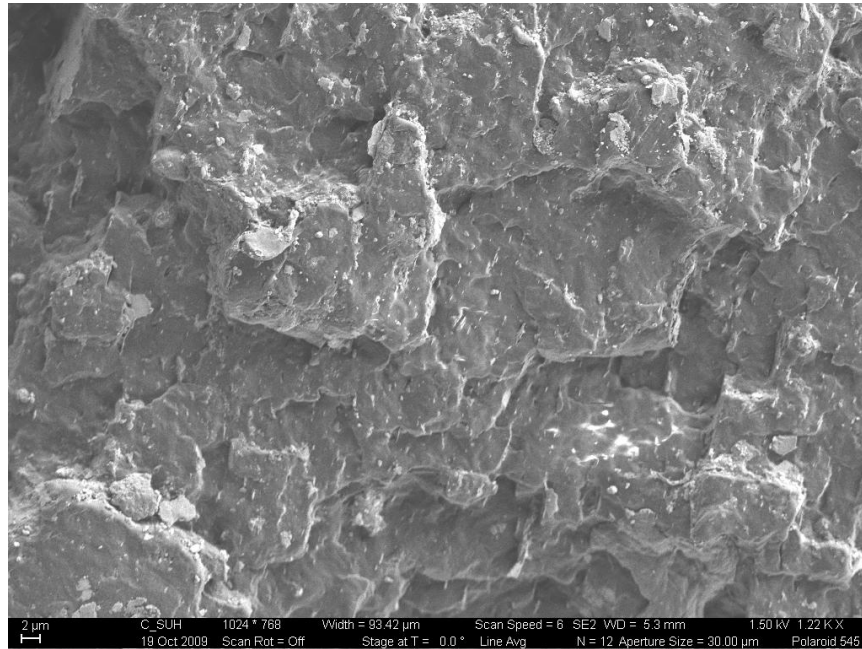


Figure 3.17 Fracture surface of 10 wt% nanokaolin-PP

### 3.5 Ashby Plots: Specific Property and Material Cost

In order to compare the performance, including cost and weight reduction, Ashby plots are used to identify the material that has the best performance in cost reduction and in property improvement relative to PP. Improvement in composite's specific property (e.g. HDT/density) and its cost were calculated and shown in the plots. According to the costs provided by LyondellBasell and XG sciences, the costs of PP, xGnP1, xGnP15, and xGnP-PP PNCs were calculated. As the cost of talc was not provided, the average cost of talc (based on online vendors) was used instead. Additionally, nanokaolin's cost is not yet commercially available, so



nanokaolin-PP is not included in the Ashby plots. A summary of the material cost is shown in Table 3.1.

Table 3.1 Material Costs

| Material         | Cost (\$/kg) |
|------------------|--------------|
| PP               | 2.11         |
| xGnP1            | 22.00        |
| xGnP15           | 11.00        |
| Talc             | 1.10         |
| 10 wt% xGnP1-PP  | 4.10         |
| 10 wt% xGnP15-PP | 3.00         |
| 10 wt% Talc-PP   | 2.01         |
| 40 wt% Talc-PP   | 1.71         |

In terms of improvement in specific flexural strength relative to PP, as shown in Figure 3.18, xGnP1-PP has demonstrated significantly better performance than xGnP15-PP, talc-PP. However, it has the highest cost among PP and all the composites. It is observed that the addition of xGnP results in higher cost and addition of talc results in lower cost. 40 wt% talc-PP has the lowest cost and higher improvement than 10 wt% talc-PP and 10 wt% xGnP15-PP, whereas 10 wt% xGnP1-PP has the highest improvement in specific flexural strength, but the sacrifice is on the cost. Lastly, 10% xGnP15-PP is a more expensive material with the lowest improvement in specific flexural strength compared to other composites.

In terms of improvement in specific flexural strength, 40 wt% talc-PP is definitely the material that should be used, as it offers the highest improvement at the lowest cost among all the composites in Figure 3.19. Although 10 wt% xGnP1-PP also has improvement higher than 10 wt% talc-PP and 10 wt% xGnP15-PP, it is the most expensive composite.

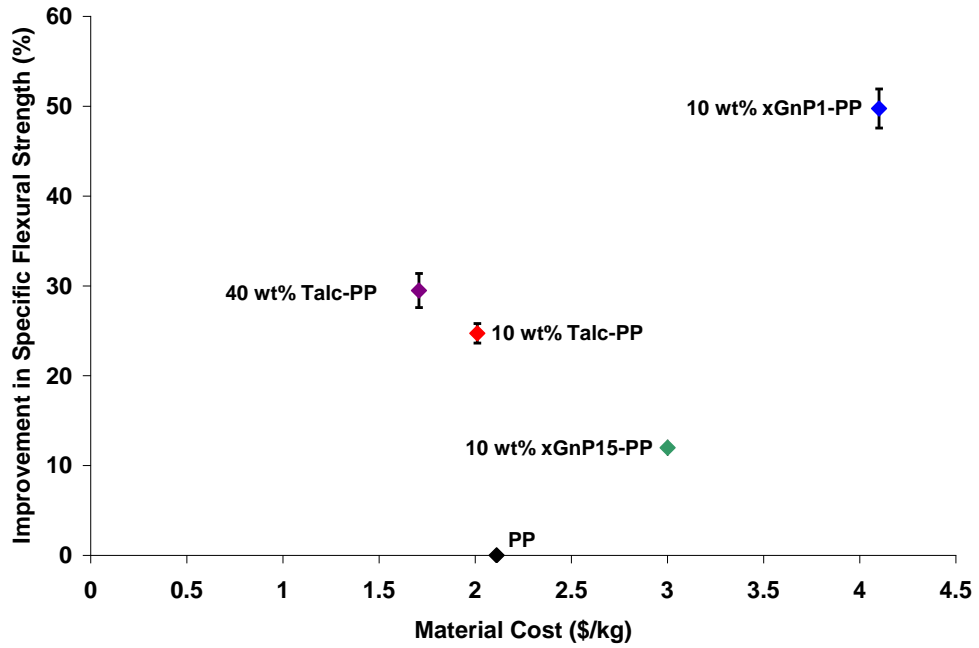


Figure 3.18 Ashby plot of specific flexural strength vs. material cost

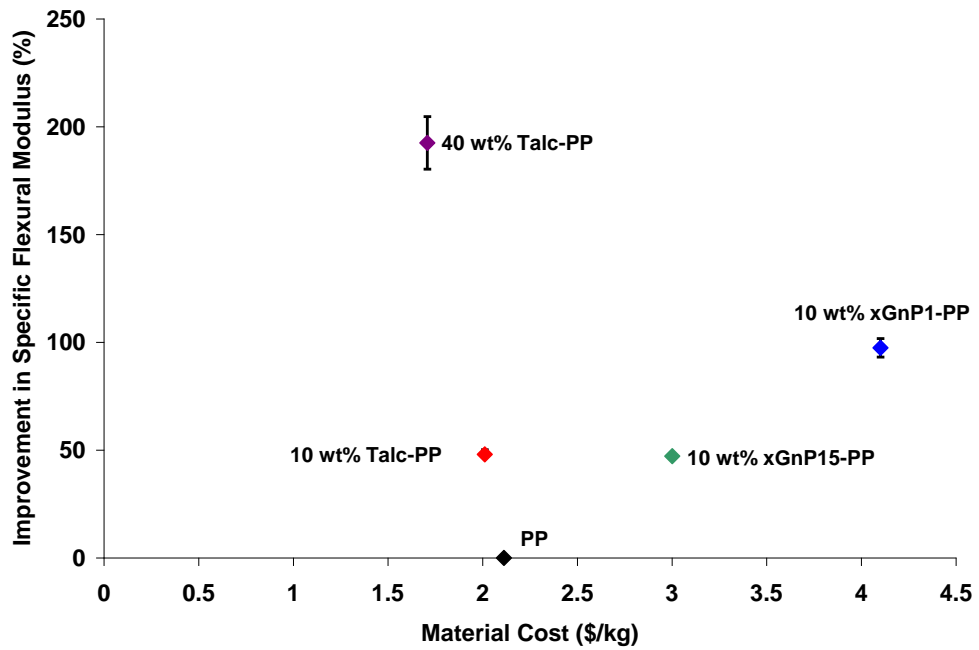


Figure 3.19 Ashby plot of specific flexural modulus vs. material cost

Figure 3.20 shows an Ashby plot in terms of improvement in specific impact strength and material cost. Even though talc composites cost significantly less than xGnP1-PP, they lead to poorer performance in specific impact strength, whereas the addition of xGnP1 results in improvement in specific impact strength relative to PP. As impact strength is the most critical property for rear bumper applications, this Ashby plot is indicating that higher cost is inevitable for higher performance in impact strength.

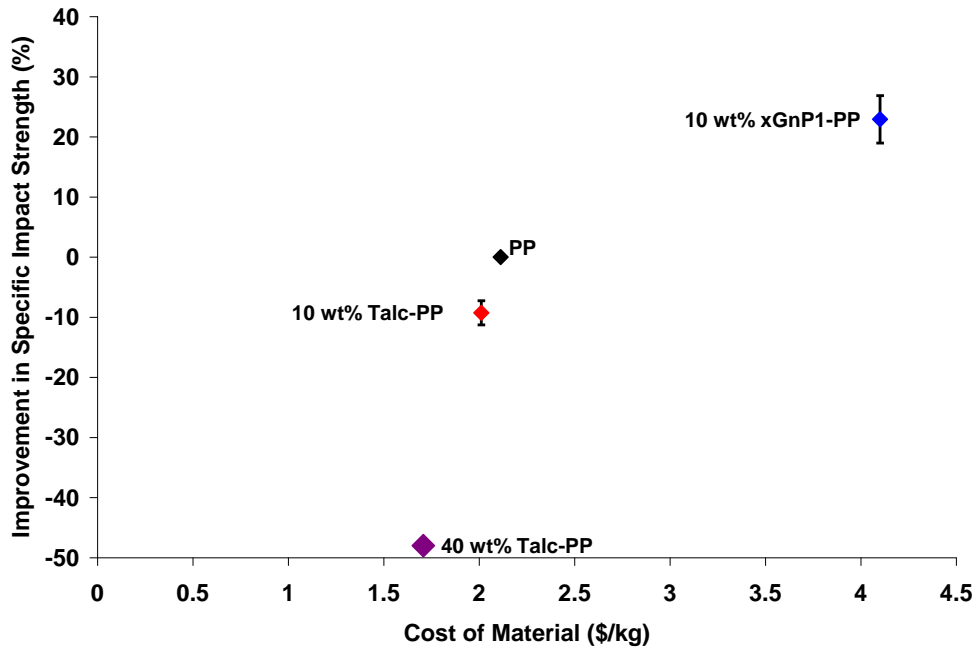


Figure 3.20 Ashby plot of specific impact strength vs. material cost

Figure 3.21 shows an Ashby plot in terms of improvement in specific HDT and material cost. The trend is similar to that in Figure 3.19. 40 wt% talc-PP results in the highest improvement in specific HDT and it has the lowest cost. Even though 10 wt% xGnP1-PP and xGnP15-PP have comparable performance to 10 wt% talc-PP in improving the specific HDT of PP, their costs are higher. From Figure 3.21, it is clear that 40 wt% talc-PP has the best performance in terms of specific HDT and material cost.

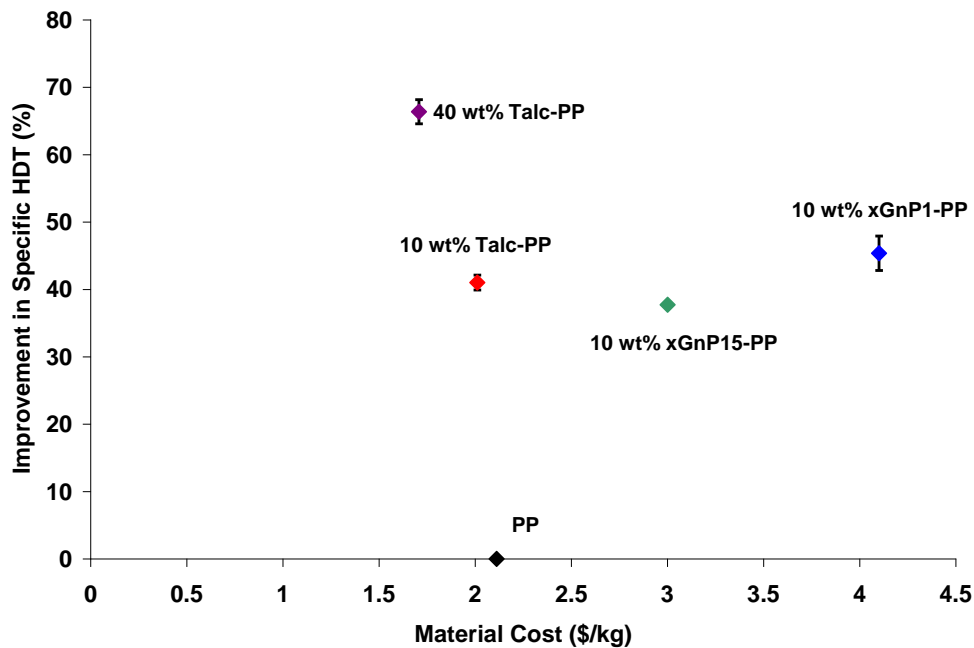


Figure 3.21 Ashby plot of specific HDT vs. material cost

Figure 3.22 shows an Ashby plot in terms of improvement in specific CLTE and composite cost. 40 wt% talc-PP, 10 wt% talc-PP, and 10 wt% xGnP1-PP are comparable in terms of improvement in specific CLTE and have overlapping error bars. However, 10 wt% xGnP1-PP is the most expensive material in the figure. 10 wt% xGnP15-PP shows the lowest improvement in specific CLTE and it has higher cost than the talc composites.

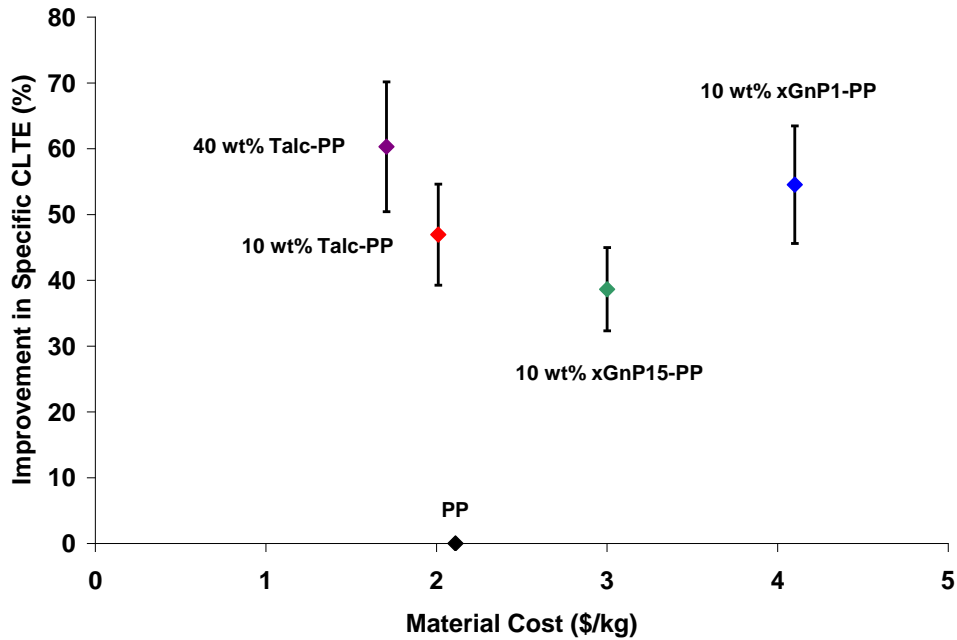

































Figure 3.22 Ashby plot of specific CLTE vs. material cost

Looking at all the Ashby plots, 40 wt% talc-PP leads to the highest improvements at the lowest cost in specific flexural modulus, specific HDT, and specific CLTE. 10 wt% xGnP1-PP leads to the highest improvements in all specific properties presented comparing at equivalent filler loading, and achieves higher improvement than 40 wt% talc-PP in specific flexural strength and specific impact strength. However, the main limitation of 10 wt% xGnP1-PP is that it is the most costly material, even though it has comparable or better performance to 40 wt% talc-PP in specific flexural strength, specific HDT and specific CLTE.

### 3.6 Summary of Results

Table 3.2 shows a comparison summary covering the performance of some representative composites in the properties characterized in this chapter. The level of improvement or declination relative to PP is indicated by arrows of varying size.

Table 3.2 Summary of composite performance in various properties

|                   | Flexural Strength   | Flexural Modulus  | Impact Strength   | HDT   | CLTE  | Stiffness   | Specific Density  | Cost  |
|-------------------|---|---|---|---|---|---|---|---|
| 10 wt% xGnP1-PP   |    |    |    |    |    |    |    |    |
| 10 wt% xGnP1 5-PP |    |    |   |    |    |    |    |    |
| 10 wt% Talc-PP    |  |  |  |  |  |  |  |  |
| 40 wt% Talc-PP    |  |  |  |  |  |  |  |  |









|                         |   |                         |   |
|-------------------------|---|-------------------------|---|
| Highest Improvement     |  | Slight Declination      |  |
| Significant Improvement |  | Moderate Declination    |  |
| Moderate Improvement    |  | Significant Declination |  |
| Slight Improvement      |  | Highest Declination     |  |

Table 3.2 indicates that the addition of any filler within PP results in improvement relative to PP in all the properties except impact strength, specific density and cost. The trends in flexural modulus, HDT, CLTE and stiffness are very similar, indicating that 40 wt% talc-PP has the best performance, followed by 10 wt% xGnP1-PP. The major achievements of 10 wt% xGnP1-PP are its highest improvement in flexural strength, impact strength and lowest increase in material density. However, it has the poorest performance in terms of material cost reduction. 40 wt% talc-PP is outstanding in most properties apart from its poor impact strength and high density, which are critical in the rear bumper application. 10 wt% xGnP15-PP generally follows the trend of 10 wt% xGnP1-PP but the level of improvements is lower in all properties except cost. For 10 wt% talc-PP, the improvements are also lower than 40 wt% talc-PP but it has lower declination in the performance of impact strength and density.

### **3.7 Conclusions**

In order to develop a multifunctional PNC for automotive applications, mechanical properties (flexural and impact), thermo-mechanical properties (HDT, CLTE, stiffness), and specific density were determined. xGnP and nanokaolin composites were compared to composites filled with talc, which is the filler currently used by Honda to make rear bumpers. The performance of xGnP1-PP and nanokaolin-PP was optimized by employing the best compounding method based on flexural properties, impact strength, and HDT. Melt mixing is the best compounding method for nanokaolin-PP, whereas the use of surfactant has a negative effect on the performance of nanokaolin-PP, and sonication and the use of compatibilizer either have no effect or a negative effect on the performance improvement compared to melt mixing. As most of the information on nanokaolin was kept confidential by the material supplier, only one

type of compatibilizer for clay was used in this study. In order to optimize the type of compatibilizer used and the amount, more research on the chemistry and properties of nanokaolin should be performed. The coating method is the best for xGnP-PP compared to melt mixing and solid state mixing using a tumbler. Addition of solid state mixing did not increase the improvement relative to melt mixing.

xGnP-PP prepared with coating method and nanokaolin-PP prepared with melt mixing were compared to talc-PP. In property comparison, flexural modulus, HDT, and CLTE share similar trends in which improvement increases with increasing filler content, and xGnP1-PP results in the highest improvement at equivalent filler loading, but 40 wt% talc-PP still has the best performance in these properties.

For a rear bumper, the most important property is the impact strength and experimental data has shown that xGnP1-PP has higher impact strength at all filler loadings and at both temperature conditions tested. Furthermore, 10 wt% xGnP1-PP also has higher flexural strength than 40 wt% talc-PP indicating that xGnP1 has the potential to replace talc in the bumper application due to its outstanding performance in impact and flexural strengths. xGnP1-PP also demonstrates high performance in thermo-mechanical properties including HDT, CLTE, and stiffness compared to nanokaolin-PP and talc-PP at 10 wt%. Finally, xGnP1-PP has the lowest specific density among all the composites at 10 wt%, which maximizes the weight reduction of parts made by xGnP1-PP.

Even though xGnP1-PP has shown great promise as a multifunctional PNC, Ashby plots have indicated that 40 wt% talc-PP still has better performance in flexural modulus, specific HDT, and specific CLTE at a cost almost 2 times lower than 10 wt% xGnP1-PP. As 10 wt% xGnP1-PP demonstrates significantly better performance in impact and flexural strengths, the



rear bumper can be made thinner with xGnP1-PP and still maintain its impact and flexural strength comparable to the current state of the art. A thinner part also means a reduction in cost and weight, which aids the cost limitation on xGnP1. It is also possible that the cost of xGnP1 will decrease if the demand rises in the future.

# **CHAPTER 4**

## **PREDICTING ELECTRICAL CONDUCTIVITY OF POLYMER NANOCOMPOSITES**

The electrical conductivity of polymeric composites is one of the most important material properties for engineering applications and there is a need for a material design tool that can predict electrical conductivity and percolation threshold. The electrical conductivity, rheological properties, and flexural properties of CB-PP, VGCF-PP, and xGnP15-PP were characterized experimentally and possible correlation between the thermo-mechanical properties and the electrical conductivity of the composites was investigated as a way to predict percolation threshold. Electrical conductivity models were investigated and evaluated through comparison with experimental data. This chapter includes presentation of experimental data from the characterization of electrical conductivity, rheological properties, and comparison between experimental data and model predictions.

### **4.1 Electrical Conductivity of Polymer Nanocomposites**

A summary of electrical conductivity results for CB-PP, VGCF-PP, and xGnP15-PP as a function of filler weight percent is shown in Figure 4.1.



It is also important to recognize that even though xGnP15 has the highest intrinsic conductivity of 18,000 S/cm, compared to 10-100 S/cm for CB and 10,000 S/cm for VGCF, xGnP15-PP has the highest percolation threshold of 20.5 wt%. Apart from the alignment effect during injection molding, xGnP15-PP tends to agglomerate especially at concentrations above 10 wt% as discussed in Chapter 3. Agglomeration of xGnP causes the nanoplatelets to overlap which means an increase in equivalent filler thickness and thus a decrease in aspect ratio, which further results in a higher percolation threshold. It is also observed that the conductivities of all three composites reach the same plateau value at high filler concentration. Therefore, it can be stated that processing methods and aspect ratio are more dominant factors than the filler's intrinsic conductivity on the composite electrical conductivity and percolation threshold.

Lastly, xGnP15-PP values of conductivity below the percolation threshold were higher than those of the other two material systems. This is because PP used for xGnP15-PP was in powder form instead of pellets, and the specimens were fabricated at different times, so there might be some cross contamination within the equipment.

## **4.2 Rheological Properties**

The results for CB-PP, VGCF-PP, and xGnP15-PP are summarized in Figure 4.2 and Figure 4.3. A general trend for all three nanocomposites is that Tan Delta starts to approach zero as filler content increases. This means that the material loses the ability to dissipate energy and its stiffness increases. Again, percolation thresholds for CB-PP, VGCF-PP, and xGnP15-PP nanocomposites were 3 wt%, 8.5 wt%, and 20 wt% respectively, based on the results from Figure 4.1, and they are indicated by the black arrows in Figure 4.2. It can be seen that Tan Delta of each nanocomposite becomes close to zero at its corresponding percolation threshold.

Therefore, if there is a way to determine when Tan Delta becomes zero, the percolation threshold of PNC can be predicted.

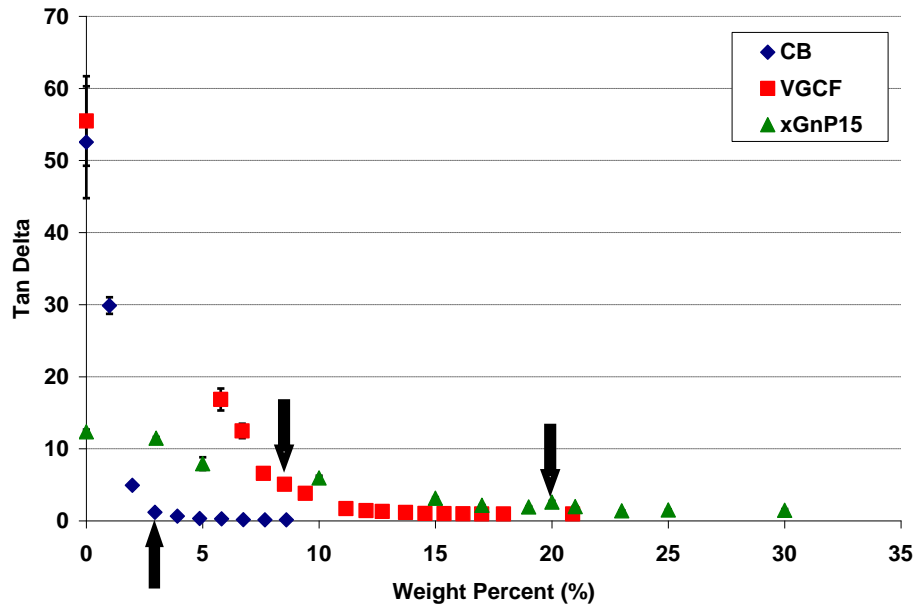


Figure 4.2 Tan Delta of CB-PP, VGCF-PP and xGnP15-PP as a function of filler weight percent

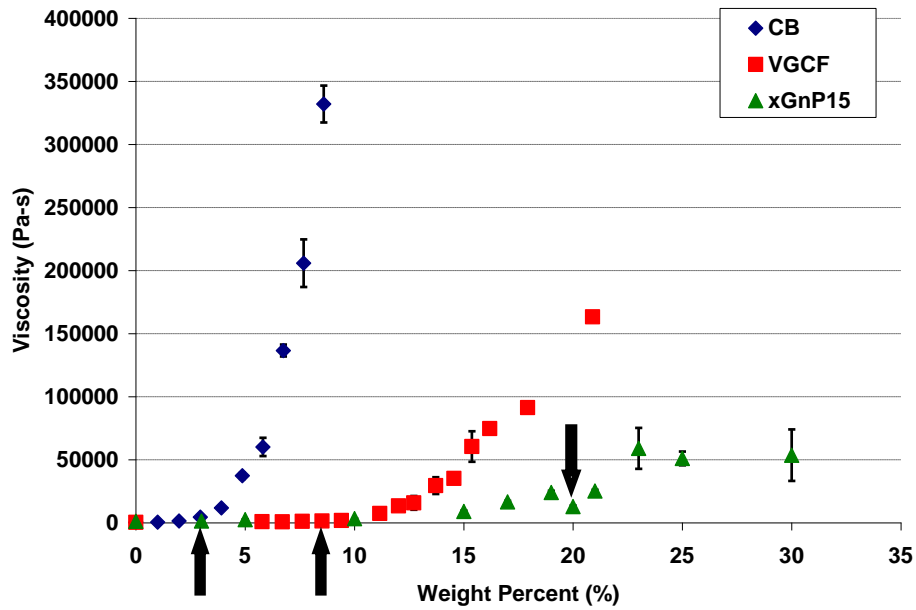


Figure 4.3 Viscosity of CB-PP, VGCF-PP and xGnP15-PP as a function of filler weight percent

Data from viscosity experiments indicate a similar trend as shown in Figure 4.3. After CB-PP, VGCF-PP, and xGnP15-PP reach their percolation thresholds as indicated by black arrows, their viscosities begin to increase significantly. This drastic increase in viscosity can be explained by the formation by the filler materials of a conductive network that confines the motion of polymer chains. However, it is generally expected that the “rheological percolation threshold” should be slightly lower than that of electrical conductivity as the distance between fillers that is required to confine the motion of polymer chains is greater than the distance required for electrons to transfer [53].

### **4.3 Flexural Properties**

Flexural strength and flexural modulus were also characterized to explore any potential correlation with percolation threshold. The results for CB-PP, VGCF-PP, and xGnP15-PP are summarized below in Figure 4.4 and Figure 4.5. Percolation thresholds are again indicated by black arrows in both figures. In Figure 4.4, the flexural strengths of these three nanocomposites generally increase as filler content increases, but they reach a plateau after a certain concentration. Although there is no clear relationship between flexural strength and percolation threshold, percolation thresholds tend to be around the transition from increasing strength to the plateau region. In Figure 4.5, the flexural moduli of all three nanocomposites basically increase with increasing filler wt% apart from two anomalous data points at 20 wt% and 25 wt% xGnP15. Therefore, no conclusion can be drawn from the flexural modulus results.

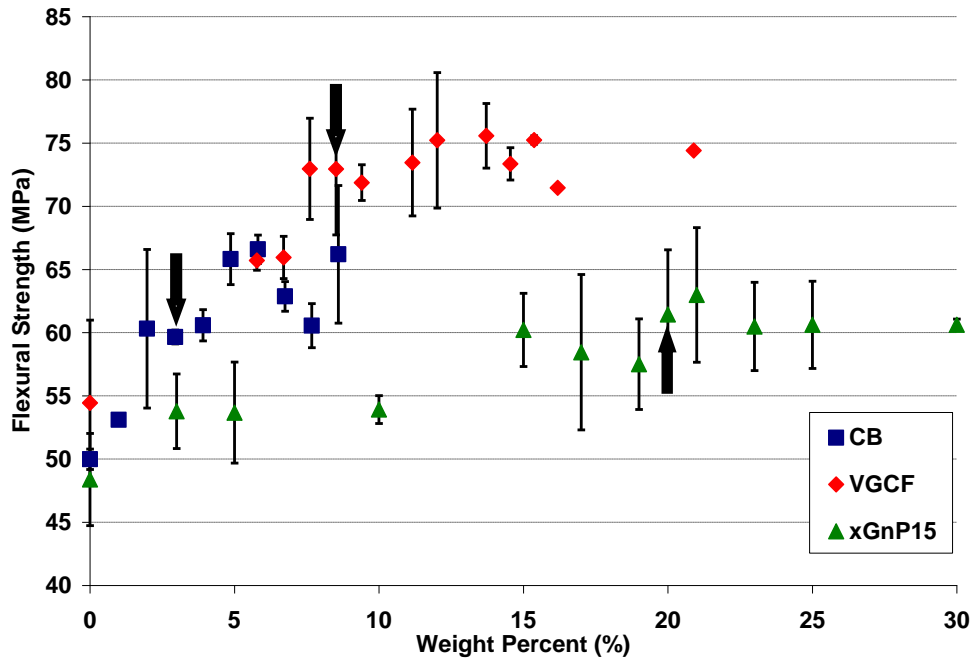


Figure 4.4 Flexural strength of CB-PP, VGCF-PP and xGnP15-PP as a function of filler weight percent

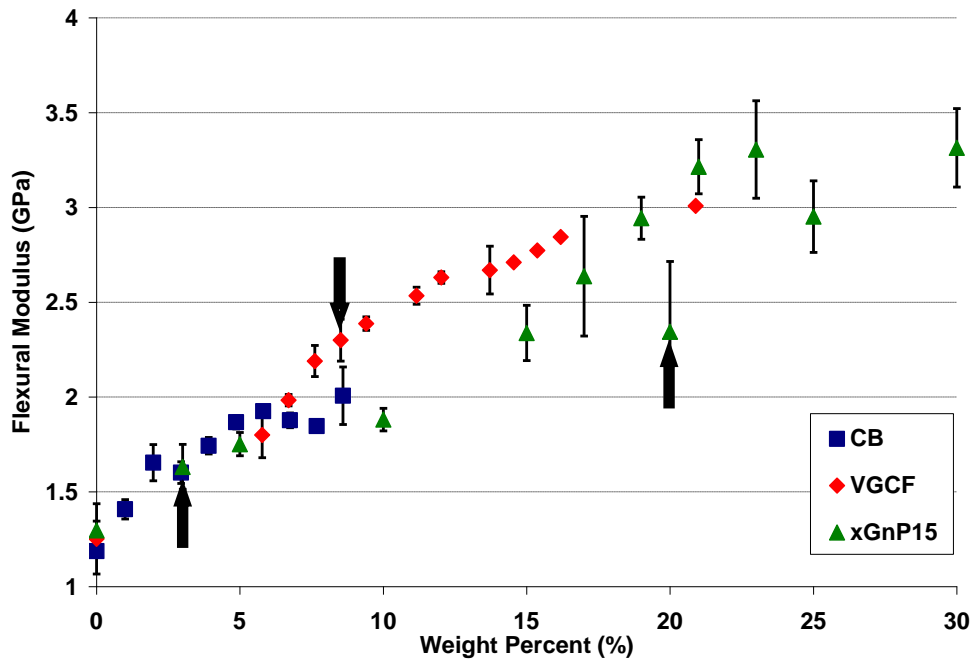


Figure 4.5 Flexural modulus of CB-PP, VGCF-PP and xGnP15-PP as a function of filler weight percent

## 4.4 Electrical Conductivity Models and Comparison to the Experimental Data

Three theoretical models for predicting electrical conductivity were studied: the percolation model, the General Effective Medium (GEM) model, and Mamunya's model. The first two are statistical models and Mamunya's model is a thermodynamic model.

### 4.4.1 Percolation Model

The percolation model is one of the earliest models proposed by Kirkpatrick [43] in 1973 and it has become the basis for development of other later electrical conductivity models. This model states that electrical conductivity may be predicted above the percolation threshold following the power law, and it is formulated in Equation 4.3,

$$\sigma_m = \sigma_f(\Phi - \Phi_c)^t \quad (4.3)$$

where  $\sigma_m$  is the composite conductivity,  $\sigma_f$  is the filler conductivity,  $\Phi$  is the filler loading vol%,  $\Phi_c$  is the percolation threshold, and  $t$  is the critical exponent.

Although the critical exponent is believed to have a universal value of 2.0 according to [54,55], there are insufficient experimental data to support this. Currently there is no standard way to determine this  $t$  value. According to the theory [55],  $t$  does not depend on the structure and geometrical properties of the system, only the system dimension.

In order to determine  $t$ , two approaches were employed in this study by means of linear fitting of the experimental data. First, the model equation as given in Equation 4.3 was rearranged into a linear form shown below,

$$\log(\sigma_m) = \log(\sigma_f) + t \log(\Phi - \Phi_c) \quad (4.4)$$

where the  $\log$  of  $\sigma_f$  represents the y-intercept,  $t$  represents the slope, percolation threshold determined from experiments was used,  $\log \sigma_m$  is the y variable and  $(\Phi - \Phi_c)$  is the x variable. In



Figure 4.6, experimentally determined  $\log \sigma_m$  was plotted as a function of  $(\phi - \phi_c)$  and a linear trend line was fitted through the data points. In the first approach, the y-intercept was set using the filler conductivity values provided by the manufacturers as listed in Chapter 2. The equations of fitting and correlation coefficients of fitting ( $R^2$ ) are also displayed in Figure 4.6.

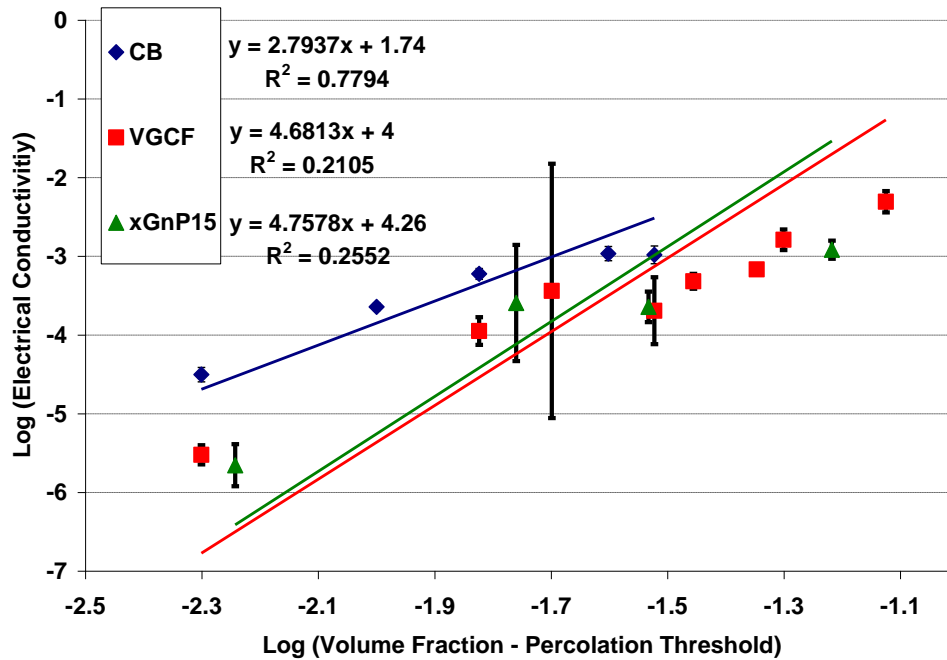


Figure 4.6 Linear fitting of experiment data with pre-set filler conductivity for percolation model

Table 4.1 shows a summary of  $t$  values obtained, correlation coefficients, and the resulting average experimental data to model prediction ratio (Exp-Model Ratio) for each nanocomposite system. “Exp-Model Ratio” is used as a criterion to evaluate the performance of a model in this study. It is an average value obtained by computing the ratio of experimental conductivity to the model prediction at each filler loading level. When the ratio is above one, it means the model under predicts; the model predictions match the data points perfectly if the ratio is 1, and the model over predicts if the ratio is below one.

Table 4.1 Comparison between experimental data and percolation model (first approach)

| <b>Filler Material</b> | <b><math>t</math></b> | <b><math>R^2</math></b> | <b>Exp-Model Ratio</b> |
|------------------------|-----------------------|-------------------------|------------------------|
| CB                     | 2.79                  | 0.7794                  | $1.027 \pm 0.104$      |
| VGCF                   | 4.68                  | 0.2105                  | $1.180 \pm 0.337$      |
| xGnP15                 | 4.76                  | 0.2552                  | $1.214 \pm 0.482$      |

The correlation coefficients from the fittings are low and indicate that the  $t$  values obtained in Table 4.1 are inaccurate. Furthermore, the resulting Exp-Model Ratios are much larger than 1 with high standard deviations especially for VGCF-PP and xGnP15-PP. Therefore, a second approach was employed to see if better results could be obtained. The second approach is similar to the first one, except the y-intercept was not pre-set when a linear trend line was fitted through experimental data points in Excel. The equations of the fitting and correlation coefficients are displayed in Figure 4.7 and Table 4.2 shows the resulting  $t$  values, correlation coefficients, Exp-Model Ratios, and filler conductivities from the linear fitting in the second approach. Exp  $\sigma_f$  are also compared to the literature values provided by the material suppliers.

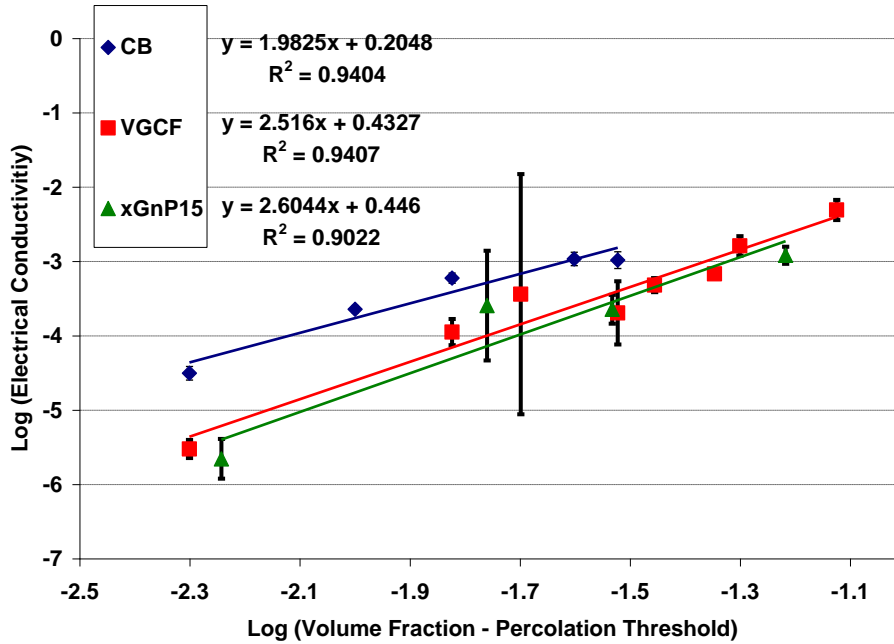


Figure 4.7 Linear fitting of experiment data without pre-set filler conductivity for percolation model

Table 4.2 Comparison between experimental data and percolation model (second approach)

| Filler Material | $t$  | $R^2$  | Exp-Model Ratio   | Exp $\sigma_f$ (S/cm) | Lit $\sigma_f$ (S/cm) |
|-----------------|------|--------|-------------------|-----------------------|-----------------------|
| CB              | 1.98 | 0.9404 | $1.000 \pm 0.046$ | 1.603                 | 55                    |
| VGCF            | 2.52 | 0.9407 | $1.000 \pm 0.065$ | 2.708                 | 10000                 |
| xGnP15          | 2.60 | 0.9022 | $1.003 \pm 0.092$ | 2.793                 | 18000                 |

In the second approach, the correlation coefficient of fitting for each nanocomposite is close to 1, and the  $t$  values obtained are somewhat close to the universal value of 2.0. Most importantly, the Exp-Model ratios are also very close to 1 with low standard deviation indicating a good agreement between experimental data and model predictions. However, the problem with this approach is that the intercepts (Exp  $\sigma_f$ ) obtained from the linear fitting differ significantly from the theoretical values (Lit  $\sigma_f$ ) as seen in Table 4.2 and it can be suggested that this model

needs an additional parameter to account for this deviation. It is noted that carbon black's  $\text{Exp } \sigma_f$  differs from  $\text{Lit } \sigma_f$  only by one order of magnitude but the differences are four orders of magnitude in the case of VGCF and xGnP. Hence, the additional parameter is probably not a fixed constant, but more likely to be related to the filler property. Since the most significant difference between CB, VGCF, and xGnP15 is their shape, and thus aspect ratio, it can be suggested that this additional parameter that should be incorporated into the percolation model is related to the aspect ratio. To verify this,  $\text{Exp } \sigma_f$  was assumed to be a function of  $\text{Lit } \sigma_f$ , filler aspect ratio, and constants, and an equation shown below was obtained by linear fitting of three data sets of  $\text{Exp } \sigma_f$  and  $\text{Lit } \sigma_f$  in Table 4.2 with a correlation coefficient of 0.9876 in Figure 4.8. The modified percolation model can be expressed by Equation 4.6.

$$\text{Exp } \sigma_f = \frac{-0.0288 \text{ Lit } \sigma_f}{\text{Aspect Ratio}} + 3.2046 \quad (4.5)$$

$$\sigma_m = \left( \frac{-0.0288 \text{ Lit } \sigma_f}{\text{Aspect Ratio}} + 3.2046 \right) (\phi - \phi_c)^t \quad (4.6)$$

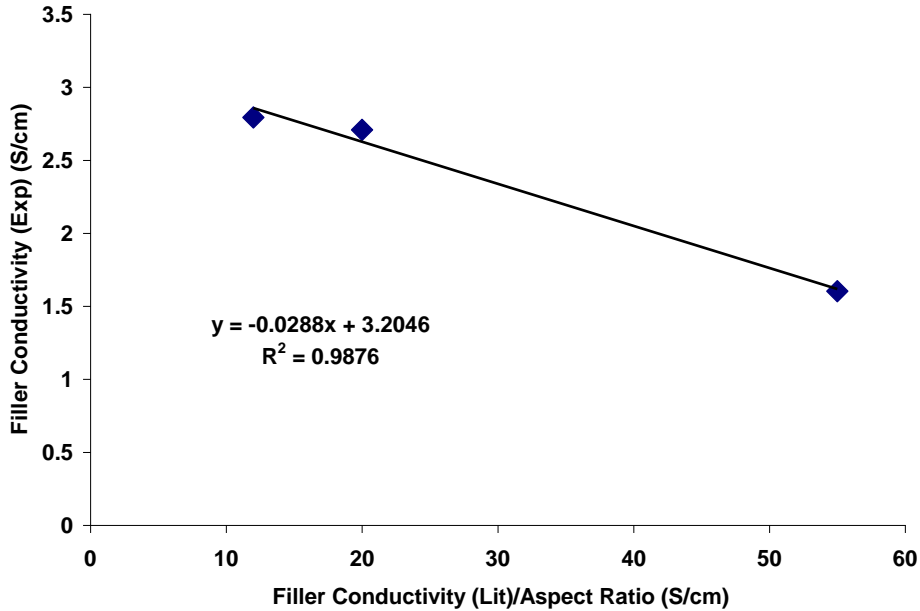


Figure 4.8 Experimental filler conductivity as a function of theoretical filler conductivity

#### 4.4.2 General Effective Medium Model

The GEM model is a statistical model developed by McLachlan [45] and its equation is given below,

$$\frac{(1-\phi)(\rho_m^{1/t} - \rho_f^{1/t})}{\rho_m^{1/t} + \left(\frac{1-\phi_c}{\phi_c}\right)\rho_f^{1/t}} + \frac{\phi(\rho_m^{1/t} - \rho_p^{1/t})}{\rho_m^{1/t} + \left(\frac{1-\phi_c}{\phi_c}\right)\rho_p^{1/t}} = 0 \quad (4.7)$$

where  $\rho_m$  is the composite resistivity,  $\rho_p$  is the polymer resistivity,  $\rho_f$  is the filler resistivity, and  $t$  is the critical exponent.  $t$  is unknown and the GEM model equation cannot be rearranged into linear form.  $t$  is determined by computing the Exp-Model Ratios over a range of  $t$  values and the  $t$  values with Exp-Model ratio closest to one were chosen. The chosen  $t$  values and the corresponding Exp-Model ratios for each nanocomposite are summarized in Table 4.3. Figure 4.9 shows the comparison between experimental data and model predictions. It is expected that none of the models applies below the percolation threshold. For this reason, it is noted that Exp-Model ratios in this case were computed based on the data points after the percolation thresholds. In addition, predicting electrical conductivity above the percolation threshold is generally more critical and is the focus for all the models.

Table 4.3 Critical exponent and experimental data to model prediction ratio for GEM model

| Filler Material | $t$ | Exp-Model Ratio |
|-----------------|-----|-----------------|
| CB              | 2.9 | 0.978 ± 0.094   |
| VGCF            | 5.3 | 0.993 ± 0.164   |
| xGnP15          | 6.7 | 0.993 ± 0.144   |

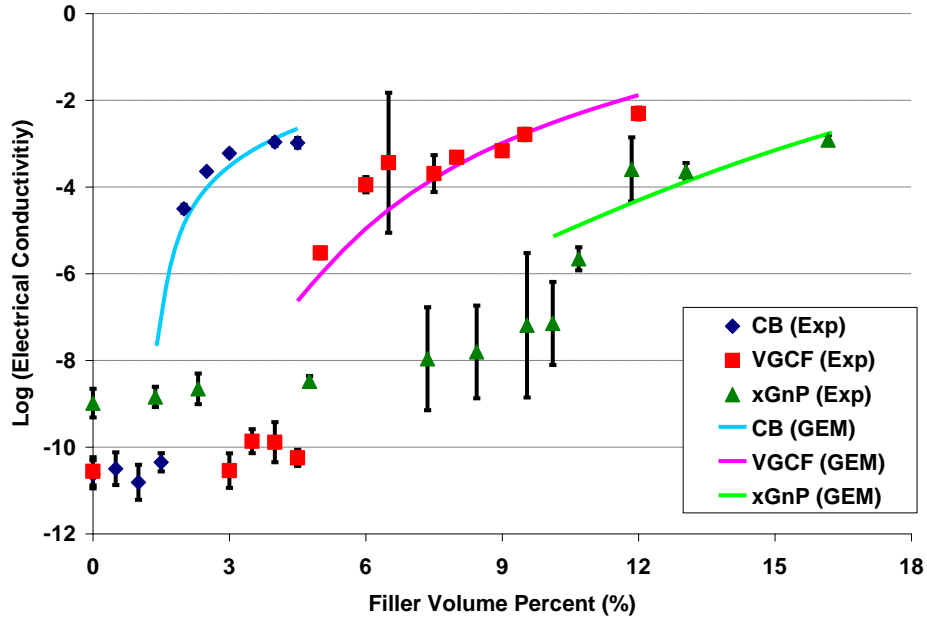


Figure 4.9 Comparison between experimental data and GEM model

Exp-Model ratios in the study of the GEM model are all close to 1 for each nanocomposite. However, it can be observed from Figure 4.9 that experimental data points are either above or below the prediction line. Another challenge with the GEM model is the arbitrarily determined  $t$ .

#### 4.4.3 Mamunya's Model

Mamunya's model is a thermodynamic model that takes into account more factors than the statistical models. Mamunya's model is defined by Equations 4.8 through 4.11 as shown in the following [34],

$$\log \sigma_m = \log \sigma_p + (\log \sigma_{max} - \log \sigma_p) \left( \frac{\phi - \phi_c}{F - \phi_c} \right)^k \quad (4.8)$$

$$k = \frac{K \phi_c}{(\phi - \phi_c)^{0.75}} \quad (4.9)$$

$$K = A - B\gamma_{pf} \quad (4.10)$$

$$\gamma_{pf} = \gamma_p + \gamma_f - 2(\gamma_p\gamma_f)^{0.5} \quad (4.11)$$

where  $\sigma_p$  is the polymer conductivity,  $\sigma_{max}$  is plateau conductivity (maximum composite conductivity),  $F$  is the max packing factor,  $A$  and  $B$  are constants,  $\gamma_{pf}$  is the surface tension between polymer and filler,  $\gamma_p$  is the polymer surface energy, and  $\gamma_f$  is the filler surface energy. For this model, the percolation threshold and the plateau conductivity are both determined from experiments; the max packing factor for CB, VGCF, and xGnP were obtained from [56-58], respectively. Due to the difficulty in obtaining surface energies for the polymer and the filler, the surface tension,  $A$ , and  $B$  are unknown. Therefore the constant  $K$  was derived by linear fitting of the experimental data. Mamunya's model equation was rearranged into the following equation in the form of  $y=Kx$ ,

$$\log \left[ \frac{(\log \sigma_m - \log \sigma_p)}{(\log \sigma_{max} - \log \sigma_p)} \right] = K \left[ \frac{\phi_c}{(\phi - \phi_c)^{0.75}} \right] \log \left( \frac{\phi - \phi_c}{F - \phi_c} \right) \quad (4.12)$$

Table 4.4 shows the  $K$  values from linear fitting, correlation coefficients and resulting Exp-Model ratios for Mamunya's model. The correlation coefficients are quite close to 1, indicating good agreement with the experimental data. Exp-Model ratios are also close to 1 with low standard deviation. A comparison between experimental data and model predictions can be seen in Figure 4.10.

Table 4.4 Comparison between experimental data and Mamunya's model

| <b>Filler Material</b> | <b>F</b> | <b>K</b> | <b>R<sup>2</sup></b> | <b>Exp-Model Ratio</b> |
|------------------------|----------|----------|----------------------|------------------------|
| CB                     | 0.11     | 0.0882   | 0.9371               | 0.968 ± 0.038          |
| VGCF                   | 0.82     | 0.0445   | 0.8776               | 1.060 ± 0.106          |
| xGnP15                 | 0.49     | 0.0282   | 0.9651               | 0.972 ± 0.065          |

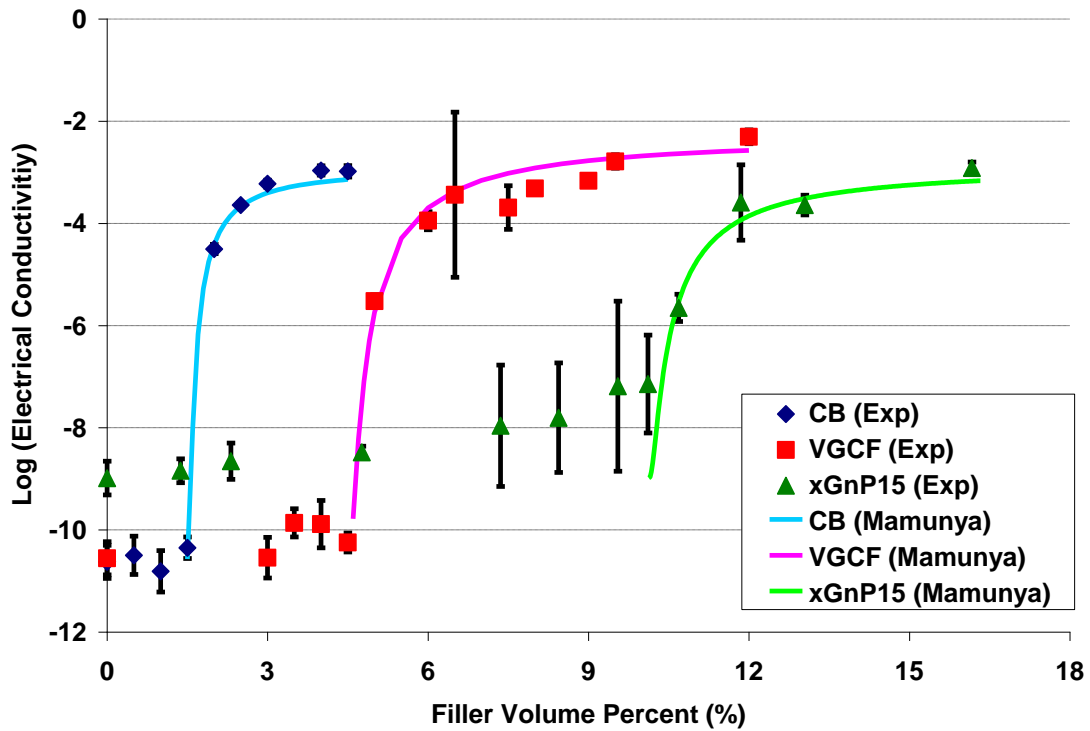


Figure 4.10 Comparison between experimental data and Mamunya's model predictions

Based on Exp-Model ratios shown in Table 4.4 and Figure 4.10, Mamunya's model predictions match the experimental data closely. Even though the performance of Mamunya's model is the best among the three electrical conductivity models studied, some of the parameters were determined based on experimental data and linear fitting, which involve arbitrariness. First, the percolation threshold and plateau conductivity have to be determined from experiments. Plateau conductivity is related but not equal to the filler conductivity, even though there may exist a way to determine plateau conductivity with an approach similar to that discussed in the percolation model section. Second, surface tension is a function of surface energies and additional experiments are required to measure the surface energy of polymer and filler. Third, A and B are unknown constants. Finally, there are no universally proven and constant values for



max packing factors  $F$ , as fillers have either complex shapes (highly structured CB) or varying aspect ratios or inconsistent dimensions.

#### **4.5 Conclusions**

The electrical conductivity, Tan Delta, viscosity, flexural strength, and flexural modulus of CB-PP, VGCF-PP, xGnP15-PP were determined as functions of filler loading level. It was discovered that the processing methods and aspect ratios of fillers have dominant effects on the electrical conductivity and the percolation threshold. Additionally, experimental results have indicated that the percolation threshold may be predicted if there are ways to determine when Tan Delta approaches zero or when viscosity starts to increase drastically. The importance of predicting the percolation threshold is that it is one of the most crucial parameters to determine in the evaluations of the electrical properties of PNCs for engineering applications. However, it is not time and cost efficient to obtain a value for the percolation threshold by fabricating and characterizing PNCs at different filler loading levels. Furthermore, most of the existing theoretical models require an input for the percolation threshold as shown by the model equations in Section 4.4.

The percolation model, the GEM model, and Mamunya's model were evaluated in terms of Exp-Model Ratios in this research study. The results indicated that the percolation model likely needs an additional parameter or function related to aspect ratio in order to produce more accurate results. Mamunya's model had the best performance among the three models in terms of Exp-Model Ratios and low standard deviations. However, much of arbitrariness was involved. Furthermore, there are some common limitations of using the percolation model, the GEM model and Mamunya's model. First, all three models require at least one experimentally

determined parameter: the percolation threshold, and plateau conductivity for Mamunya's model. Second, critical exponents in the percolation model and the GEM model, parameter  $K$  (Equation 4.10) in Mamunya's model were determined based on some arbitrariness. Last but not least, all three models do not account for all the factors that affect electrical conductivity such as manufacturing methods and the presence of interphase [59].

## CHAPTER 5

### CONCLUSIONS AND SUGGESTIONS FOR FUTURE WORK

#### 5.1 Research Conclusions

The demand for PNCs has been increasing in the automotive industry due to superior properties. PNCs are multifunctional in structural, thermal, and electrical applications, and offer potential in cost reduction and weight reduction. Body panels, step-assists, seat backs, engine parts, and tires are examples of PNC usage in automotive applications. Furthermore, PNCs reinforced with conductive fillers enable the application of electrostatic painting on products and eliminate the need for primer. However, it is difficult to determine the percolation threshold and the amount of filler required for a specific electrical conductivity value because there is lack of a design tool that can predict electrical conductivity of PNCs accurately.

With all the mentioned motivation, advantages and limitations, the goal of this study is to develop PNCs for automotive applications by optimizing manufacturing methods, and by characterization of mechanical properties, thermo-mechanical properties, specific density, and electrical conductivity.

In material selection, PP homopolymer was used as the polymer matrix, and xGnP-PP and nanokaolin-PP were compared to talc-PP for Honda's rear bumper application. In the first phase of this study, xGnP1-PP and nanokaolin-PP prepared by various compounding methods were fabricated. The compounding methods include melting mixing, solid state mixing with a tumbler, coating with sonication, the use of surfactants, and the use of compatibilizer. Their performance in mechanical properties and HDT were characterized to identify the compounding method that optimized PNC performance. Experimental data indicated that xGnP1-PP prepared

with the coating method and nanokaolin-PP prepared with melt mixing resulted in the highest performance and they were compared to talc-PP. The comparison was primarily performed between 10 wt% PNCs and 40 wt% talc-PP because 40 wt% talc-PP is the current state of the art for rear bumper application. Furthermore, increasing filler content usually leads to improvement in composite performance but agglomeration is likely to have negative impact on composite performance and it is also cost prohibitive for filler loading higher than 10wt %.

Comparison between xGnP1-PP, xGnP15-PP, nanokaolin-PP and talc-PP indicated that xGnP1 exhibited promising performance as a multifunctional PNC for automotive applications, especially in terms of flexural strength, impact strength, HDT, CLTE, stiffness, and specific density. It has the additional advantage of being electrically conductive compared to talc and nanokaolin. More specifically, xGnP1-PP has significantly better performance than talc-PP in flexural and impact strengths, which are the most critical properties for rear bumper application. The low density xGnP1-PP can also offer additional weight reduction in the rear bumpers. However, even if 10 wt% xGnP1-PP has better or comparable performance to 40 wt% talc-PP, the main limitation is the cost of xGnP1.

As xGnP has the advantage of being electrically conductive, this study also has an emphasis on electrical conductivity. One of the major challenges in the fabrication of electrically conductive PNCs is the lack of design tools that can accurately predict electrical conductivity and percolation threshold. The most traditional method is to measure electrical conductivity as a function of filler loading. However, this method is inefficient as fabrication and characterization of materials often require significant amounts of time and cost. This study aims to predict the electrical conductivity or percolation threshold of PNCs with three approaches: finding correlations between material properties, and investigation of theoretical models. CB, VGCF,

and xGnP were chosen for their difference in filler shape for investigation of the effects of aspect ratio on electrical conductivity and percolation threshold. More specifically, xGnP15 was used over xGnP1 for its higher aspect ratio.

Electrical conductivity, flexural properties, Tan Delta and dynamic viscosity of CB-PP, VGCF-PP, xGnP15-PP were determined as functions of filler content. It was discovered that processing methods and aspect ratio of fillers have dominant effects on electrical conductivity and percolation threshold. There was no definite correlation between flexural properties and electrical conductivity or percolation threshold. However, correlation was discovered between the percolation threshold and rheological properties, such that Tan Delta and viscosity of PNCs would go through a drastic change at the point of percolation threshold. If Tan Delta and viscosity can be predicted by using theoretical models in literature, then this can provide an indirect way to determine the percolation threshold without fabrication of composites. However, this still requires time and cost for all the material fabrication and characterization.

Three electrical conductivity models, the percolation model, the GEM model and Mamunya's model were studied for comparison to experimental results. The results from the analysis of these theoretical models showed reasonable performances in terms of Exp-Model ratios but indicated some limitations at the same time. First, all of the models studied require an input for percolation threshold, but currently there is no definite and accurate way other than experimentation to determine it. This is one of the purposes for finding correlations between rheological properties. Second, the models often have arbitrary constants involved, such as the critical exponents  $t$  in statistical models and numerical constants  $A$  and  $B$  in Mamunya's thermodynamic model. Again, it is not efficient to use a model if any parameter has to be derived from experimental data. Lastly, none of the models studied accounts for the manufacturing

methods that have effects on the dispersion and orientation of fillers. The use of injection molding has shown that the orientation of fillers has significant impact on the percolation threshold of a PNC. Therefore, existing electrical conductivity models should be modified such that they would require minimum arbitrariness and would account for all the factors involved in electrical conductivity.

## **5.2 Suggestions for Future Work**

As the major limitation of xGnP1-PP is its cost, additional sources of graphite at a cheaper cost should be identified. Additionally, it has been discussed previously that the manufacturing process has effects on the orientation and dispersion of fillers, and therefore on the electrical conductivity and the percolation threshold. Experimental data from Chapter 4 has also shown that VGCF-PP had higher percolation threshold than that of CB-PP due to the use of injection molding. Therefore, CB-PP, VGCF-PP and xGnP15-PP can be fabricated by compression molding instead of injection molding and can be characterized for examination of the effects of compression molding on electrical conductivity and percolation threshold. It is expected that VGCF-PP, and xGnP15-PP would have lower percolation threshold with compression molding, as discussed in section 1.3.2 in Chapter 1. The same procedure can be performed for electrical conductivity models to see how the use of compression molding will affect the parameters in the model.

## REFERENCES

1. Koo, J. H. (2006). Polymer nanocomposites: processing, characterization, and applications, The McGraw-Hill Companies, Inc.
2. R. A. Vaia (2003). "Polymer Nanocomposites Open a New Dimension for Plastics and Composites." The AMPTIAC Newsletter, **6**(1): 17-24.
3. Polymer Nanocomposites Synthesis, Characterization and Modeling, R. Krishnamoorti, and R. A. Vaia, eds., American Chemical Society, Symposium Series 804, Washington, DC (2001)
4. Advani, S. G. (2007). Processing and Properties of Nanocomposites. Singapore, World Scientific Publish Co. Pte. Ltd.
5. Serope Kalpakjian, S. R. S. (2008). Manufacturing processes for engineering materials, Pearson Education.
6. Wu, S. H. (1988). "A generalized criterion for rubber toughening- the critical matrix ligament thickness." *J. Appl. Polym. Sci.* **35**(2): 546-561.
7. Wei Zhang, A. A. D.-S., Richard S. Blackburn (2007). "Carbon based conductive polymer composites." Journal of Materials Science **42**(10): 3408-3418.
8. Domoff, D. J. (2009). "Automotive Plastics." *Plastics Engineering* 65(8).
9. T. Kurauchi, A.Okada, T.Nomura, T.Nishio, S.Saegusa, R.Deguchi, SAE Technical Paper Ser, 910584 (1991)

10. Lloyd, S. M. and L. B. Lave (2003). "Life Cycle Economic and Environmental Implications of Using Nanocomposites in Automobiles." Environmental Science & Technology **37**(15): 3458-3466.
11. Dillon, D. R., K. K. Tenneti, et al. (2006). "On the structure and morphology of polyvinylidene fluoride–nanoclay nanocomposites." Polymer **47**: 1678-1688.
12. R. Leaversuch, "Nanocomposites Broaden Roles in Automotive, Barrier Packaging", Plastics Technology, Online Article can be found in <http://www.ptonline.com/articles/200110fa3.html> (as of June 30<sup>th</sup> 2010)
13. L. M Sherman, "Chasing Nanocomposites", Plastics Technology, Online Article can be found in <http://www.ptonline.com/articles/200411fa2.html> (as of June 30<sup>th</sup> 2010)
14. <http://www.worldcarfans.com/104102110118/hummer-h2-sut-sports-lightweight-nanocomposite-material> (as of July 15<sup>th</sup> 2010)
15. <http://www.carbonmotors.com/press#images> (as of June 30<sup>th</sup> 2010)
16. Carbon Motors Corporation. (2008). "Carbon Motors™ Selects Soliant's Fluorex® Paintfilm for its Exterior Body Panels", Multimedia can be found in <http://www.carbonmotors.com/news-releases/40/Carbon-Motors-Selects-Soliant's-Fluorex-Paintfilm-for-its-Exterior-Body-Panels> (as of June 30<sup>th</sup> 2010)
17. Myers, A. W. U.S. Department of Energy Inventions & Innovation Program Final Report.
18. [http://two-wheels.michelin.com/2w/fron/index.jsp?codePage=2092004115340\\_21032005140627&codeRubrique=2092004115340&lang=EN](http://two-wheels.michelin.com/2w/fron/index.jsp?codePage=2092004115340_21032005140627&codeRubrique=2092004115340&lang=EN) (as of May 25<sup>th</sup> 2010)



19. Burton, D. (2006). Enabling Electrostatic Painting of Automotive Polymers with Low Cost Carbon Nanofibers.
20. <http://owners.acura.com/Maintenance/InCaseOfAccident.aspx?link=all> (as of June 30<sup>th</sup> 2010)
21. Rakesh K. Gupta, E. K., Kwang-Jea Kim (2010). Polymer Nanocomposites Handbook, CRC Press, Talyor & Francis Group.
22. Gul', V. E. (1996). Structure and properties of conducting polymer composites, VSP BV.
23. J. Larminie, A. D. (2003). Fuel Cell Systems Explained, John Wiley & Sons, Ltd. New York, 2003.
24. G.O. Mepsed, J.M. Moore, Handbook of Fuel Cells—Fundamentals, Technology and Application, John Wiley and Sons, Ltd., New York, 2003, pp. 286–293.
  - a.
25. Kulikovsky, A. A. (2006). "Voltage loss in bipolar plates in a fuel cell stack." Journal of Power Sources **160**(1): 431-435.
26. Yang, T. and P. Shi (2008). "Study on the mesocarbon microbeads/polyphenylene sulfide composite bipolar plates applied for proton exchange membrane fuel cells." Journal of Power Sources **175**(1): 390-396.
27. K. RoBberg, V. Trapp, Handbook of Fuel Cells—Fundamentals, Technology and Applications, John Wiley & Sons, Ltd., New York, 2003, pp. 308–314.
  - b.
28. Dhakate, S. R., R. B. Mathur, et al. (2007). "Properties of graphite-composite bipolar plate prepared by compression molding technique for PEM fuel cell." International Journal of Hydrogen Energy **32**(17): 4537-4543.

29. Liao, S.-H., C.-C. Weng, et al. (2010). "Preparation and properties of functionalized multiwalled carbon nanotubes/polypropylene nanocomposite bipolar plates for polymer electrolyte membrane fuel cells." Journal of Power Sources **195**(1): 263-270.
30. Gokturk, H. S., T. J. Fiske, et al. (1993). "Effects of particle shape and size distributions on the electrical and magnetic properties of nickel/polyethylene composites." Journal of Applied Polymer Science **50**(11): 1891-1901.
31. Fiske, T., H. Gokturk, et al. (1997). "Percolation in Magnetic Composites." Journal of Material Science **32**: 5551-5560.
32. Yi, J. Y. and G. M. Choi (1999). "Percolation Behavior of Conductor-Insulator Composites with Varying Aspect Ratio of Conductive Fiber " Journal of Electroceramics **3**(4): 361-369.
33. Jing, X., W. Zhao, et al. (2000). "The effect of particle size on electric conducting percolation threshold in polymer/conducting particle composites " Journal of Materials Science Letters **19**(5): 377-379.
34. Mamunya, E. P., V. F. Shumskii, et al. (1994). "Rheological Properties and Electric Conductivity of Carbon Black-Filled Polyethylene and Polypropylene." Polymer Science **36**(6): 835-838.
35. M. Weber, M. R. Kamal. (1997). "Estimation of the volume resistivity of electrically conductive composites." Polymer Composites **18**(6): 711-725.
36. Advani, S. G. and C. L. T. III (1987). "The Use of Tensors to Describe and Predict Fiber Orientation in Short Fiber Composites." Journal of Rheology **31**(8): 751-784.
37. Kazuya, N., I. Hitoshi, et al. (1998). "Effect of particle size of graphites on electrical conductivity of graphite/polymer composite " Composite Interfaces **6**(5): 483-495.

38. Fiske, T., H. S. Gokturk, et al. (1997). "Effects of flow induced orientation of ferromagnetic particles on relative magnetic permeability of injection molded composites." Polymer Engineering & Science **37**(5): 826-837.
39. Yaguchi, H., H. Hojo, et al. (1995). "Measurement of Planar Orientation of Fibers for Reinforced Thermoplastics Using Image Processing." International Polymer Processing(3): 262-269.
40. Yin, Y., T. J. Mays, et al. (1989). "The measurement of grain orientations in an extruded electrode graphite using image analysis." Carbon **27**(1): 113-115.
41. Broadbent, S. R. and J. M. Hammersley (1957). "Percolation processes." Mathematical Proceedings of the Cambridge Philosophical Society **53**(3): 629-641.
42. Lux, F. (1993). "Models proposed to explain the electrical conductivity of mixtures made of conductive and insulating materials " Journal of Materials Science Letters **28**(2): 285-301.
43. Kirkpatrick, S. (1973). "Percolation and Conduction." Rev. Mod. Phys. **45**(4): 574-588.
44. Zallen, R. (1983). The Physics of Amorphous Solids, John Wiley & Sons.
45. McLachlan, D. S., M. Blaszkiewicz, et al. (1990). "Electrical Resistivity of Composites." Journal of the American Ceramic Society **73**(8): 2187-2203.
46. K. Kalaitzidou, H. Fukushima, and L. T. Drzal. (2007). "A New Compounding Method for Exfoliated Graphite-Polypropylene Nanocomposites with Enhanced Flexural Properties and Lower Percolation Threshold." Composite Science and Technology **67**: 2045-2051.

47. Sung J.H. and H.J. Choi (2004). "Electrorheological Characteristics of Poly(o-ethoxy)aniline Nanocomposite." Korea-australia Rheology Journal **16**(4): 193-199.
48. Trung, V.Q. and D.N. Huyen (2009). "Synthesis, Properties and Application of Polyindole/TiO<sub>2</sub> Nanocomposites." Journal of Physics: Conference Series **187**.
49. Gorai, S. and S. Chaudhuri (2006). "Optical characterization of In<sub>2</sub>S<sub>3</sub>-SiO<sub>2</sub> nanocomposite thin films synthesized by sol-gel technique." Materials Science and Engineering: B **126**(1): 97-101.
50. K. Kalaitzidou, H. Fukushima, L. T. Drzal, (2007). "Mechanical Properties and Morphological Characterization of Exfoliated Graphite-Polypropylene Nanocomposites." Applied Science and Manufacturing **38**: 1675-1682.
51. K. Kalaitzidou, H. Fukushima, L. T. Drzal. (2007). "Multifunctional Polypropylene Composites Produced by Incorporation of Exfoliated Graphite Nanoplatelets." Carbon **45**: 1446-1452.
52. <http://webmineral.com/data/Talc.shtml> (as of Aug 15<sup>th</sup> 2010)
53. Du, F., R. C. Scogna, et al. (2004). "Nanotube Networks in Polymer Nanocomposites: Rheology and Electrical Conductivity." Macromolecules **37**: 9048-9055.
54. Derrida, B., D. Stauffer, et al. (1983). "Tunneling and Nonuniversal Conductivity " Physical Review Letters **59**(12): 1305-1308.
55. Stauffer, D. (1985). Introduction to Percolation Theory. London, Taylor and Francis.
56. LEE, B.-L. (1992). "Electrically Conductive Polymer Composites and Blends." Polymer Engineering & Science **32**(1): 36-42.

57. Kuriger, R. J. and M. K. Alam (2002). "The electrical properties of polymer nanocomposites with carbon nanotube fillers." Experimental Heat Transfer **15**: 19-30.
58. Drzal, L. T. (2006). Exfoliated Graphite Nanoplatelets (xGnP) A Carbon Nanotube Alternative for Modifying the Properties of Polymers and Composites, Michigan State University, online presentation can be found in [http://www.xgsciences.com/about/xGnP\\_tech\\_overview\\_web.pdf](http://www.xgsciences.com/about/xGnP_tech_overview_web.pdf) (as of July 15<sup>th</sup>)
59. Seidel, GD, and DC Lagoudas (2009). "A Micromechanics Model for the Electrical Conductivity of Nanotube-Polymer Nanocomposites." Journal of Composite Materials **43**(9) :917-941.